Electron scattering from argon: Data evaluation and consistency

E. Gargioni* and B. Grosswendt

Physikalisch-Technische Bundesanstalt, 38116 Braunschweig, Germany

(Published 2 April 2008)

The demand for coherent scattering data for modeling electron transport in matter has increased in recent years. While much effort has been devoted to the improvement of models describing electron transport and scattering, the updating of fundamental data sets on the basis of recent experimental results has often been neglected. The use of a well-validated set of electron cross sections ensures accurate calculations of transport parameters and ionization yields, with typical applications in material analysis, detector response studies, plasma diagnostics, physics of the atmosphere, and radiotherapy. Data consistency can be verified on the basis of various theoretical requirements, and systematic errors can be minimized by cross-checking results obtained from independent experiments. For example, the oscillator strength distribution of an atom can be obtained both from photoabsorption experiments and from zero-angle electron-atom collisions at high energy, on the basis of the Bethe theory. A considerable number of all electron-scattering experiments are concerned with light noble gases, in particular with argon. This gas is a dominant constituent of noble-gas discharge plasmas and plays an important role in rare-gas halide lasers and proportional scintillator counters. This work reviews electron-scattering cross sections and optical data for the argon atom, discusses the progress made in the field of electron scattering and photoabsorption, and focuses on the most appropriate criteria for verifying data consistency.

DOI: 10.1103/RevModPhys.80.451 PACS number(s): 32.70.Cs, 32.80.Fb, 34.80.Bm, 34.80.Dp

CONTENTS

I. Introduction 451
A. Most relevant on-line data sources 452
B. Definition of cross sections in electron-atom collisions 453
1. Single-collision experiments 453
2. High-energy collisions and photoabsorption 453
3. Low-energy collisions and swarm experiments 454
II. Experimental Techniques 455
A. Beam experiments 455
1. Crossed-beam technique 455
2. Energy-loss spectroscopy 456
3. Static-gas techniques 457
4. Optical emission measurements 457
B. Swarm techniques 458
C. Photoabsorption and photoionization techniques 459
III. Theoretical Background 460
A. General calculation methods 460
B. Analytical formulas for inelastic cross sections 462
IV. Consistency Requirements for Cross-Section Data 462
A. Primary requirements 462
B. High-energy requirements 462
C. Optical data and sum rules requirements 462
V. Data Analysis 463
A. Optical oscillator strengths 463
1. Discrete transitions 464
2. Continuum region 464
3. Sum rules 465
B. Elastic cross sections 465
1. Momentum transfer and viscosity cross sections 468
C. Excitation cross sections 469
1. Optically allowed states 469
2. Optically forbidden states 471
3. Comparison with earlier data on total excitation 471
D. Ionization cross sections 472
1. Differential ionization cross sections 473
2. *K*-shell ionization 473
E. Total scattering cross section 475
VI. Concluding Remarks 475
Acknowledgments 478
Appendix A: Argon Energy Levels and Binding Energies 478
Appendix B: Tables for Oscillator Strengths 478
References 478

*elisabetta.gargioni@ptb.de

I. INTRODUCTION

Accurate electron-scattering cross sections are of crucial importance when studying electron transport in matter and are needed in many areas of applied physics. These areas include radiation dosimetry, surface electron spectroscopy, plasma physics, astrophysics, and physics of the atmosphere. In addition, the scattering of electrons is important for determining the structure of atoms and molecules, which can be excited by electron impact to optically forbidden levels.

The literature on electron scattering by atoms and molecules is very extensive as experiments and theoretical studies have been carried out for more than a century. A few early studies are still relevant today and provide deep insight into the fundamental aspects of

experiments and theoretical methods, even if some of the results are outdated. This applies, for instance, to the surveys of Kieffer and Dunn (1966), Moiseiwitsch and Smith (1968), and Bederson and Kieffer (1971) concerning ionization, excitation, and total electron scattering, respectively. Recently, Trajmar and McConkey (1994) dealt with the general issue of producing benchmark measurements of cross sections for electrons. They also analyzed the principles of electron-single-scattering experiments used for determining integral and differential cross sections and illustrated examples of data analysis and consistency checks. Crompton (1994) discussed instead the characteristics of swarm experiments, the basic concepts of solving the Boltzmann equation, and the problems related to the determination of accurate electron transport data. We believe, therefore, that the reader interested in studying electron transport through matter can find enough information in the literature on how to set up reliable experiments or undertake theoretical studies. New, consistent, and complete sets of data are needed, however. In fact, one of the major problems in electron transport studies is the large uncertainty in fundamental data, such as differential and integral cross sections. For this reason, instead of reviewing all existing experimental results, we focus on the most important criteria for building up accurate compilations.

Progress has been made in the past few years not only in measuring and collecting reliable data but also in setting up and maintaining easily accessible on-line databases. For example, Gallagher (1994) and McDaniel and Mansky (1994) provided helpful descriptions of the role of data centers and some practical discussions on how to locate and assess the required information. Moreover, the reviews of Zecca *et al.* (1996) and Inokuti *et al.* (2000) on electron collisions with atoms represent an important contribution in synthesizing reliable data. Zecca *et al.* produced selected sets of experimental cross sections for total electron scattering and Inokuti *et al.* compiled a series of data related to electron interactions with atoms, molecules, and their ions, but without focusing on data analysis issues. Other reviews surveyed mostly experimental methods or theoretical models for a specific type of process. Bell *et al.* (1983), Märk *et al.* (1995), and the International Commission on Radiation Units and Measurements (ICRU, 1996) focused on electron-impact ionization cross sections, while Heddle and Gallagher (1989) considered the most important methods for measuring electron-impact excitation of atoms and analyzed the data by means of a number of consistency checks.

A considerable number of all electron-scattering experiments are concerned with light noble gases, in particular with argon. Noble gases, having an electronic closed-shell structure, are important test systems for various theoretical models. Moreover, since target preparation with light noble gases is straightforward, the quality of available data is generally good, thus providing reference values for determining the instrumental response in electron-scattering experiments. An important review in this field was given by de Heer *et al.* (1979), who evaluated in a semiempirical way total, elastic, excitation, and ionization cross sections for the scattering of electrons by Ne, Ar, Kr, and Xe in the energy range 20 eV–3 keV. This work, although outdated, was used as a basis for later compilations, such as those of Zecca *et al.* and Inokuti *et al.* Furthermore, the comprehensive report of Hayashi (2003), collecting an extensive bibliography of electron and photon cross sections for argon (more than 1900 references), provides a set of recommended electron-impact cross sections in the energy range 0.01 eV–1 keV that were compiled in 1992. These examples emphasize once more the need for new, comprehensive, and consistent data syntheses. Therefore, we believe it is timely and appropriate to review the progress made in the field of experimental electron scattering and to provide up-to-date compilations of elastic and inelastic cross sections.

Given the important role played by the close relationship that exists between photoabsorption and fast electron-atom collisions in the data analysis, part of this work is devoted to photoionization cross sections and optical oscillator strengths for transitions from the ground state of the argon atom.

We surveyed the literature and electronic databases accessible through the internet and focused on the most appropriate methods that can be used as criteria to verify the consistency of the experimental results in the impact energy range from a few tenths up to several thousands of eV. Although we refer only to argon, the selected procedure is general and applies to all atoms.

A. Most relevant on-line data sources

Numerical and bibliographic information on collision cross section and photoionization data can be obtained from many on-line sources. Our search of on-line data was carried out during the compilation of argon cross sections using websites of a few institutions that provide updated links to data centers and bibliographic databases. The Weizmann Institute of Science (Israel), for example, maintains a website (http://plasma-gate.weizmann.ac.il) with links to the most important databases and atomic and plasma physics institutions in the world. The Japanese National Institute of Fusion Science (NIFS, http://amdata.nifs.ac.jp with free access, https://dbshino.nifs.ac.jp for registered users only) provides numerical data and bibliographic information on electron cross sections for ionization, excitation, and recombination. The Atomic and Molecular Data Unit of the International Atomic Energy Agency (IAEA, http://www-amdis.iaea.org) maintains a numerical database (ALADDIN) in collaboration with other institutions, such as the Controlled Fusion Atomic Data Center at Oak Ridge National Laboratory (ORNL, http://www-cfadc.phy.ornl.gov). Moreover, the IAEA maintains a bibliographic database (AMBDAS) on atomic and molecular collision and radiative processes and hosts GENIE (General Internet search engine, http://www-amdis.iaea.org/GENIE), an engine that allows a multiple search of different databases on the web for spectral and collisional atomic data. The Physics Laboratory's web-

site of the National Institute of Standards and Technology (NIST) (http://physics.nist.gov) has links to all NIST physical reference data. Among other things, it is possible to access the atomic spectra database, the XCOM photon cross-section database, and the FFAST x-ray form factor, attenuation, and scattering tables. Electron-impact cross sections for ionization and excitation are also available for some atoms and molecules. From the NIST websites, it is also possible to order, free of charge, a CD containing their electron elastic-scattering cross-section database (http://www.nist.gov/srd/nist64.htm), developed by Jablonski *et al.* (2002).

B. Definition of cross sections in electron-atom collisions

1. Single-collision experiments

In a typical single-collision experiment, a homogeneous, well-collimated beam of monoenergetic electrons is directed toward a target containing scatterers. It is usually assumed that experimental conditions have been chosen so that each target scatterer acts as if it were alone and that no appreciable interactions occur among electrons. After collision, some or all electrons emerging from the interaction region are registered by detectors, usually placed at a very large distance from the scattering region. We consider a process in which an electron, with mass m_e, charge $-e$, and momentum $\hbar\boldsymbol{k}_0$, collides with an atom or molecule containing N electrons and having the nuclear charge Z, initially in the ground state ψ_0 with energy $E_0=0$. After scattering, the electron will have a momentum $\hbar\boldsymbol{k}_n$ and the target will be left in the final state ψ_n, with energy E_n. In the case of elastic scattering, the atom or molecule will remain in its ground state ψ_0, and in the case of ionization, one or more secondary electrons will be ejected from the target. Under these assumptions, the electron-atom scattering process can be described by the steady-state equation

$$H\Psi(q_0,q_1,\ldots,q_N) = \epsilon\Psi(q_0,q_1,\ldots,q_N). \tag{1}$$

Here H is the $(N+1)$-electron Hamiltonian of the system and $q_i=(\boldsymbol{r}_i,s_i)$ denotes the ensemble of the spatial coordinates $\boldsymbol{r}_i$ and spin variables s_i of atomic electron i; ϵ is the total energy of the electron-target system.

If H is a Schrödinger Hamiltonian, the electron-atom interaction potential includes only the electrostatic interactions of the projectile with both atomic electrons and the nuclear charge. This description is sufficient unless one of the following conditions applies: (i) the scattering system contains heavy atoms, (ii) spin-orbit effects are significant, or (iii) the incident projectiles have velocities near the speed of light. In the case of incident electrons traveling at relativistic speeds, it is appropriate to use the Bethe-Born approximation to treat the dynamics and to estimate cross-section values from those evaluated at lower kinetic energies [as described by Inokuti (1971)]. In general, however, it will be necessary to solve the Dirac equation, since electrons are attracted by the Coulomb field of the nucleus and can reach large velocities at small radial distances, where spin-orbit and target-polarization effects are significant. In this case, the nonrelativistic Hamiltonian must be corrected by adding terms that take these effects into account.

For a detector that subtends at the scattering center a small solid angle $d\Omega$ and is placed in the direction (θ,ϕ), we can define the differential cross section $d\sigma/d\Omega$ for a given type of scattering (elastic or inelastic) as the ratio between the flux of particles scattered per unit time into $d\Omega$ and the incident flux.

The integrated cross section is calculated using

$$\sigma(T) = \int_0^{2\pi}\int_0^{\pi} \frac{d\sigma}{d\Omega}\sin\theta\, d\theta\, d\phi. \tag{2}$$

Information about the energy spectrum and the angular distribution of secondary electrons after ionization is contained in the double-differential cross section $d^2\sigma_i/\, d\Omega\, dE$, where E is the energy of secondary electrons. The differential ionization cross section with respect to the scattering angle is then expressed by

$$\frac{d\sigma_i}{d\Omega} = \int_0^{(T-B_1)/2} \frac{d^2\sigma_i}{d\Omega\, dE} dE,$$

where B_1 is the binding energy of the valence electron. To obtain the energy spectrum of secondary electrons, the double-differential ionization cross section is integrated over the solid angle,

$$\frac{d\sigma_i}{dE} = \int_0^{2\pi}\int_0^{\pi} \frac{d^2\sigma_i}{d\Omega\, dE}\sin\theta\, d\theta\, d\phi. \tag{3}$$

The integrated cross section for ionization can therefore be obtained as

$$\sigma_i(T) = \int_0^{(T-B_1)/2} \frac{d\sigma_i}{dE} dE. \tag{4}$$

2. High-energy collisions and photoabsorption

For sufficiently fast collisions, the influence of the incident particle on an atom may be regarded as a sudden and small external perturbation. It is then reasonable to solve Eq. (1) using an approach based on the first Born approximation, since exchange effects between target and incident particles become increasingly less important as the incident particle energy increases (Bransden and Joachain, 2003). An electron impinging on an atomic target is considered to be fast if its velocity is much higher than the mean orbital velocity of atomic electrons. The differential cross section for a collision in which an electron is scattered with momentum change $\hbar\boldsymbol{K}=\hbar(\boldsymbol{k}_n-\boldsymbol{k}_0)$ and the atom is excited to a state n is then given by (Inokuti, 1971)

$$d\sigma_n = \frac{4\pi a_0^2}{T/R}\frac{\mathcal{F}_n(K)}{E_n/R} d\ln(Ka_0^2)^2. \tag{5}$$

In this equation, T is the electron kinetic energy, $a_0 = 5.292\times10^{-11}$ m is the Bohr radius, $R=13.606$ eV is the Rydberg energy, and E_n is the excitation energy of the state n measured from the ground state. The solid angle

element $d\Omega = \sin\theta\, d\theta\, d\phi$ is replaced by $\pi d(K^2)/k_n k_0$. $\mathcal{F}_n(K)$ is the generalized oscillator strength for a transition from the ground state (denoted by 0) to the state n,

$$\mathcal{F}_n(K) = (E_n/R)(Ka_0)^{-2}\left|\sum_j (n|\exp(i\boldsymbol{K}\cdot\boldsymbol{r}_j)|0)\right|^2, \tag{6}$$

where $\boldsymbol{r}_j$ is the coordinate vector of the jth atomic electron and $(n|\,|0)$ denotes a matrix element, related to the transition probability of the system from the ground state to the state n.

By expanding the exponential of Eq. (6) into a power series, one can show that

$$\lim_{K\to 0} \mathcal{F}_n(K) = f_n, \tag{7}$$

where f_n is the optical dipole oscillator strength,

$$f_n = (E_n/R)M_n^2 = (E_n/R)a_0^{-2}\left|\sum_j (n|x_j|0)\right|^2. \tag{8}$$

The optical dipole oscillator strength determines the intensity of a radiative transition for an excited atom after photoabsorption. Since the limit $K\to 0$ is approached for forward scattering at high velocities, Eq. (7) shows that there is a close relationship between a fast collision and photoabsorption.

If the transition to the state n is optically allowed, the excitation cross section obtained by integrating Eq. (5) in the limit $K\to 0$ is given by the Bethe asymptotic formula

$$\sigma_n(T) = \frac{4\pi a_0^2}{T/R}\frac{f_n}{E_n/R}\ln\left(\frac{4c_nT}{R}\right). \tag{9}$$

The constant c_n is given by

$$\ln[c_n(E_n/R)^2] = \int_0^{(Ka_0)_{\max}} \frac{\mathcal{F}_n(K)}{f_n} d\ln(Ka_0)^2 - \int_{(Ka_0)_{\min}}^{0}\left(1-\frac{\mathcal{F}_n(K)}{f_n}\right) d\ln(Ka_0)^2. \tag{10}$$

Equation (9) indicates the possibility of verifying the validity of experimental data from two independent types of measurement. The availability of experimental optical oscillator strengths allows, in fact, the determination of the inelastic electron cross sections at high energies, and vice versa (Inokuti, 1971).

If the transition to the state n is optically forbidden, then $f_n=0$ and the Bethe asymptotic cross section becomes

$$\sigma_n(T) = \frac{4\pi a_0^2}{T/R} b_n, \tag{11}$$

where b_n is a constant defined by

$$b_n = \int_{(Ka_0)_{\min}}^{(Ka_0)_{\max}} \frac{\mathcal{F}_n(K)}{E_n/R} d\ln(Ka_0)^2. \tag{12}$$

For transitions into the continuum (ionization), the single-differential cross section $d\sigma_i/dE$ is defined by an equation similar to Eq. (9),

$$\frac{d\sigma_i}{dE} = \frac{4\pi a_0^2}{T/R}\left[\frac{R}{E}\frac{df}{dE}\ln\left(\frac{4c_ET}{R}\right)\right]. \tag{13}$$

In this case, the optical oscillator strength f_n is replaced by the differential optical oscillator strength df/dE. Similarly, c_E can be defined by Eq. (10), replacing f_n with df/dE.

For an atom, the differential cross section can be integrated over the continuum energy E to obtain the ionization cross section,

$$\sigma_i = \frac{4\pi a_0^2}{T/R}\left[M_i^2\ln\left(\frac{4c_iT}{R}\right)\right], \tag{14}$$

where

$$M_i^2 = \int_0^{(T-B_1)/2}\left(\frac{R}{E}\frac{df}{dE}\right)dE \tag{15}$$

and

$$M_i^2\ln c_i = \int_0^{(T-B_1)/2}\left(\frac{R}{E}\frac{df}{dE}\right)\ln c_E dE. \tag{16}$$

When a photon of energy larger than B_1 is absorbed by an atom, the atom is ionized by ejecting one or more electrons. Photoionization cross sections can be used to obtain the oscillator strength density of atoms for energies above the ionization potential (Fano and Cooper, 1968; Kim, 1975). In fact, the photoionization cross section $\sigma_{\rm ph}$ is proportional to df/dE,

$$\sigma_{\rm ph}(E) = 4\pi\alpha a_0^2 R(df/dE), \tag{17}$$

where $\alpha\simeq 1/137$ is the fine-structure constant. This enables one to treat data on $\sigma_{\rm ph}$ and df/dE as equivalent.

3. Low-energy collisions and swarm experiments

Swarm experiments are designed to measure the macroscopic properties of an ensemble ("swarm") of electrons released in a low-pressure neutral gas under the influence of an electric field $\vec{\mathcal{E}}$. The presence of the electric field causes electrons in the gas to drift with an average velocity (the drift velocity) v_d. In general, diffusion becomes anisotropic and can be characterized by a longitudinal diffusion coefficient D_L and a lateral diffusion coefficient D_T. These transport parameters can be measured as functions of the applied electric field. In swarm experiments, the scattering is multicollisional, thus allowing the determination of scattering cross sections from transport data using statistical methods. The collision cross sections are in fact related to the transport coefficients through the Boltzmann transport equation, in which the electron ensemble is described by a time-dependent probability distribution function $F\equiv F(\vec{r},\vec{v},t)$,

reflecting the statistical nature of the macroscopic behavior of electrons due to a large number of individual interactions (Crompton, 1994),

$$\frac{\partial F}{\partial t} + \vec{v} \cdot \vec{\nabla}_r F + \vec{a} \cdot \vec{\nabla}_v F = C(F). \tag{18}$$

The Boltzmann equation gives the evolution of F in terms of its space and velocity gradients ($\vec{\nabla}_r$ and $\vec{\nabla}_v$, respectively), of the acceleration $\vec{a}=-e\vec{\mathcal{E}}/m_e$ produced by the applied electric field, and of collisions with the gas, represented by the collision operator $C(F)$. The collision operator contains information on cross sections and energy loss for each process. The electron number density $n_e(\vec{r},t)$ is given by the integral of $F(\vec{r},\vec{v},t)$ over all velocities,

$$n_e(\vec{r},t) = \int F(\vec{r},\vec{v},t)d\vec{v}.$$

Swarm techniques for determining electron collision cross sections are best applied in the low-energy range (up to a few eV), where beam experiments become increasingly difficult. The quantities that play an important role in describing electron-atom collision processes at such low energies are the momentum transfer cross section σ_m and the viscosity cross section σ_v. In the case of elastic scattering only, these quantities are related to the differential cross section as follows:

$$\sigma_m(T) = 2\pi \int_0^\pi \frac{d\sigma}{d\Omega}(1-\cos\theta)\sin\theta\, d\theta, \tag{19}$$

$$\sigma_v(T) = 2\pi \int_0^\pi \frac{d\sigma}{d\Omega}(1-\cos^2\theta)\sin\theta\, d\theta. \tag{20}$$

Momentum transfer and viscosity cross sections are important not only for determining electron transport parameters (see Sec. II.B), but also for studying gas properties (e.g., viscosity), using kinetic theories or fluid mechanics (see Žigman and Milić, 1988; Macrossan and Lilley, 2003; Sebastian and Wadehra, 2005). These studies have applications, for example, in plasma physics, semiconductor processing, and in the development of gas detectors for particle physics (where electric-discharge phenomena play an important role).

II. EXPERIMENTAL TECHNIQUES

In this section, we describe the most common experimental methods in use to determine electron-scattering cross sections and optical data for atoms and molecules. This topic has been a matter of extensive discussion in the literature, therefore we outline here only the salient aspects directly related to our data evaluation.

A. Beam experiments

Electron-impact experiments in conditions of single scattering (also called beam experiments) are carried out with an apparatus consisting schematically of an electron gun with electrostatic focusing and collimating devices, a target containing the atoms to be studied and the setup to detect and analyze scattered electrons (Bederson and Kieffer, 1971; Bransden and Joachain, 2003). Since the electron-impact energy usually spans from a few to several thousands of eV, the detailed design of the gun varies from experiment to experiment. In the case of monoatomic gases, such as argon, the target may consist of a cell containing the sample gas (static-beam technique), or it may be an atomic beam intersecting the electron beam in a small region of space (crossed-beam technique). Electrons scattered from the interaction region are then analyzed and measured at a given angle. The velocity of electrons can be selected by deflecting their paths with electrostatic fields of known characteristics. The velocity, and therefore the scattered electron current, is consequently measured.

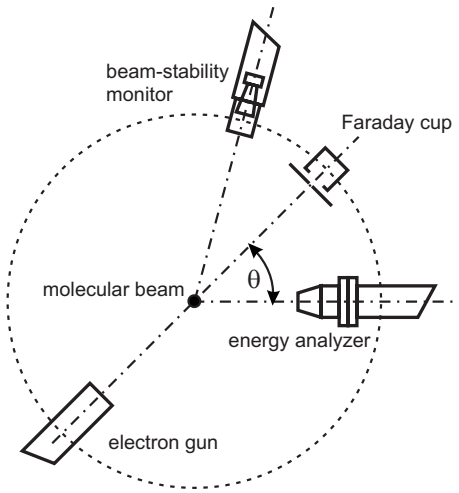

FIG. 1. Example of experimental setup for a crossed-beam experiment. The molecular (or atomic) beam is directed perpendicularly to the page. In this setup, the energy analyzer and a beam-stability monitor rotate about the collision center and the Faraday cup is used to measure the beam attenuation (see text for more details). Adapted from Grosswendt and Baek, 2000.

Electron-impact processes can also be used for measurements of excitation cross sections using optical techniques, as discussed in Sec. II.A.4.

1. Crossed-beam technique

The most frequently used technique to measure differential cross sections is the crossed-beam technique (see, for example, Fite and Brackmann, 1958; Bederson and Kieffer, 1971). The gas beam effuses from a capillary array nozzle and interacts with the electron beam inside a vacuum chamber. The electron gun, or the analyzer, rotates about the collision center. Figure 1 shows a typical setup for measuring differential cross sections with the crossed-beam technique.

Suppose that the electron beam is monoenergetic and that the velocities of molecules in the gas beam are neg-

ligible compared to the velocity of electrons. Assuming only single scattering, which is realistic if the gas pressure is sufficiently low, the absolute differential cross section is related to the measured intensity of the scattered electron according to (Bederson and Kieffer, 1971)

$$I_e(\theta,\phi)d\Omega = \frac{d\sigma}{d\Omega}d\Omega\int_V \eta(\theta,\phi;x,y,z) \times J_e(x,y,z)n_b(x,y,z)dV. \quad (21)$$

Here I_e is the number of scattered electrons per unit time, η is the transmission efficiency of the analyzer-detector system, J_e is the flux of electrons crossing the unit area located in dV, and n_b is the density distribution of the target gas in dV.

The overlap integral, which represents the extent of coverage between the electron and target beams within V and Ω, is defined as

$$F(\theta,\phi) = \int_V \eta(\theta,\phi;x,y,z)J_e(x,y,z)n_b(x,y,z)dV. \quad (22)$$

The evaluation of the overlap integral is one of the major difficulties in determining the differential cross section, because the quantities η, J_e, and n_b are generally known only approximately. Therefore, the crossed-beam technique is usually limited to relative measurements of the cross section. In this case, the data are scaled into absolute values by means of the relative-flow technique or by normalization with respect to well-known experimental or theoretical cross sections. The relative-flow technique, which is commonly used in crossed-beam experiments, employs a measurement of the ratio between the scattered intensity I_1 of the gas to be investigated and the scattered intensity I_2 of an accurately characterized gas (usually helium or nitrogen), which has a cross section that is known from absolute measurements (Srivastava *et al.*, 1975). If the incident electron beam, the scattering conditions, and the detector efficiency are kept constant during the measurements in the gases, and if no collisions occur during the gas flow in the capillary array, the ratio of the two cross sections can be expressed as follows:

$$\frac{d\sigma_1/d\Omega}{d\sigma_2/d\Omega} = \frac{I_1}{I_2}\frac{p_2}{p_1}, \quad (23)$$

where p_1 and p_2 are the pressures of the gases behind the capillary array. For a collisional flow, which represents the majority of experimental conditions, Eq. (23) is still valid, but care must be taken to ensure that the mean free paths between collisions in the capillary array are nearly identical for the reference gas and for the gas to be measured.

Recently, a new method has been developed by Grosswendt and Baek (2000) to overcome the difficulties related to the determination of the overlap integral. With this method, the double-differential cross section is defined as follows:

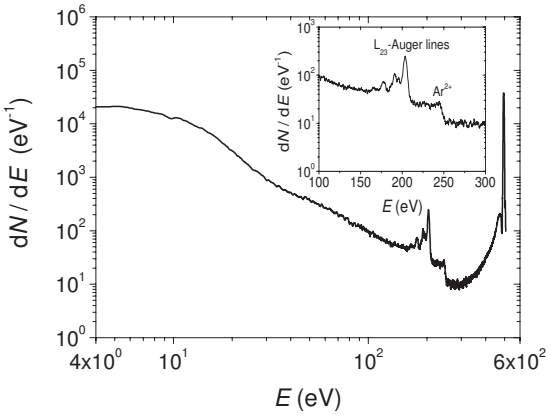

FIG. 2. Energy-loss spectrum measured in an electron collision experiment for argon as a function of the electron energy E. In this example, T=500 eV. The Auger electrons emitted after ionization of the L shell can also be observed. Figure courtesy of W. Y. Baek (PTB).

$$\frac{d^2\sigma}{dEd\Omega} = \frac{I_e(E,\theta,\phi)}{I_0(T)\,\eta(E)(\mathcal{N}l)_{\text{mean}}\Delta E\Delta\Omega}, \quad (24)$$

where $(\mathcal{N}l)_{\text{mean}}$ is the average number of target atoms or molecules per unit area along the direction of the primary electron beam inside the interaction region. ΔE represents the energy range accepted by the analyzer and $\Delta\Omega$ the corresponding solid angle. The measurement of $(\mathcal{N}l)_{\text{mean}}$ gives a very good approximation of the overlap integral and can be performed using the Lambert-Beer law:

$$(\mathcal{N}l)_{\text{mean}} = \frac{\ln[I_0(T)/I_e(T)]}{\sigma_{\text{tot}}(T)}. \quad (25)$$

The beam attenuation is measured using a Faraday cup, as shown in Fig. 1, and the total cross section $\sigma_{\text{tot}}(T)$ is determined by measuring the attenuation of a narrow electron beam of energy T as a function of the number density of atoms or molecules in a scattering chamber of well-defined dimensions (see Baek and Grosswendt, 2003). With this method, it is possible to measure absolute values of $d^2\sigma/dE\,d\Omega$, ensuring the traceability to absolute values of σ_{tot}.

The integrated cross sections, defined by Eq. (2), are calculated after extrapolating the experimental data to angles in the proximity of 0° and 180°, where measurements, due to technical difficulties, are often not possible. The extrapolation, which is generally performed either via phase shift analysis [as described in atomic physics books, such as Bransden and Joachain (2003)] or via least-squares fitting with analytical functions, can lead to significant uncertainties in the integrated cross section.

2. Energy-loss spectroscopy

With the analyzer set to accept electrons of zero energy loss, it is possible to detect the electron current due to elastic scattering (see Fig. 2). As the energy-loss set-

ting is increased, only a background of stray electrons is observed until the transmitted energy-loss component corresponds to the first excitation potential. In this configuration, the electron current has a peak. Peaks corresponding to excitation to higher states can be distinguished depending on the energy resolution of the instrument. Each peak is related to the direct excitation cross section of the corresponding state, without any complications due to cascading or to the lifetime of the excited state (as discussed in Sec. II.A.4). In practice, however, there are difficulties in applying this method to the measurement of excitation cross sections as a function of energy because of the necessity of collecting data at many angles as well as over a range of energies.

The energy-loss spectrum is analyzed taking into account the resolution properties of the experimental apparatus. The detected signal S is given by

$$S(T,\theta,E) = \int_{-\infty}^{\infty} I_e(T,\theta,E')F(E-E')dE' + B(T,\theta,E,\rho,I_0), \tag{26}$$

where I_e is the scattered electron current per steradian at electron energy E', $F(E-E')$ is the response function characterizing the effective resolution of the spectrometer, and B is the background contribution to the measured signal. The function B depends on the electron impact energy T, scattering angle θ, energy E, gas density ρ, and incident current I_0. The determination of the scattered electron current requires application of an unfolding procedure, and this can contribute significantly to the experimental uncertainty (Cartwright *et al.*, 1977).

The energy-loss spectroscopy at zero momentum transfer ($K \simeq 0$) can also be used to determine the oscillator strength distribution of atoms (Chan *et al.*, 1991), following Eq. (13). The electron energy transfer E is in fact analogous to the incident photon energy $E_\nu = h\nu$. One advantage of energy-loss spectroscopy is that it can overcome most of the problems affecting photoabsorption experiments, such as pressure effects (see Sec. II.C). Moreover, the method is straightforward if the electron-impact energy T is high when compared to the energy loss and if the scattering angle is close to zero degrees. Another approach, used, for instance, by Li *et al.* (1988), is to measure the electron energy-loss spectrum for several values of T and K and to determine the generalized oscillator strength $\mathcal{F}_n(K)$. The optical oscillator strength is then obtained by extrapolating the data to $K \to 0$ [see Eq. (7)].

3. Static-gas techniques

The static-gas technique can be used to measure both elastic and inelastic cross sections, although in elastic-scattering experiments the crossed-beam technique has been preferred in recent years (see Table III in Sec. V.B).

A static-gas apparatus to measure partial as well as total ionization cross sections is based on a parallel-plate vacuum chamber filled uniformly with the gas (of density ρ) to be measured. The electron beam is directed through the chamber, along a distance L, and usually collected in a Faraday cup. The ions produced along the path L are driven toward the detection system by means of an electric field. The measurement of the ionization cross section involves the determination of the quantities in the following relation:

$$I_i(T)/I_e(T) = \rho L \sum_{n=1}^{Z} n\sigma_i^{n+}(T) = \rho L \sigma_i(T). \tag{27}$$

Here I_i is the positive ion current generated by single-electron impact, I_e is the current of incident electrons of energy T, and σ_i^{n+} is the cross section for producing an ion of positive charge n in the collision. When all charge states are included in the sum of Eq. (27), the total (or gross) ionization cross section σ_i can be determined. Despite the conceptual simplicity of this apparatus, obtaining all quantities needed to solve Eq. (27) with good accuracy constitutes a severe problem (Kieffer and Dunn, 1966). For example, care should be taken so that (i) the number of electrons produced during the gas ionization is much smaller than the primary electron current, (ii) ions produced outside the collection region are not collected, and (iii) the parameters influencing the gas density (such as temperature and pressure) are carefully controlled.

The measurement of partial ionization cross sections requires an apparatus equipped with a system that separates ionization components of different charge and mass. This is typically implemented using time-of-flight measurements, quadrupole mass spectrometry, or energy analyzers. With these methods, Eq. (27) is modified as follows:

$$I_i^{n+}(T)/I_e(T) = \rho L \sigma_i^{n+}(T). \tag{28}$$

The determination of I_i^{n+} demands accurate knowledge of the apparatus detection efficiency for each charged species.

4. Optical emission measurements

When a monoenergetic electron beam passes through a target, some target atoms are excited into higher levels and eventually decay by emitting light. The light wavelength depends on the exact upper state that becomes populated. There are two ways to populate an excited state, namely, (i) through direct excitation from the ground state, and (ii) through a cascade from excitation into higher-lying levels. Note that the cross sections for exciting a spectral line may be different from those for exciting an atomic level. The difference between line and level excitation cross sections lies in potential population of the level by cascades from higher-energy states and the branching ratio for radiative decay of that level by transitions other than the one observed (see Fig. 3).

A typical experimental apparatus to assess the excitation cross sections by measuring optical emissions is shown in Fig. 4 [for a comprehensive discussion on optical techniques, see, for example, Filippelli *et al.* (1994)].

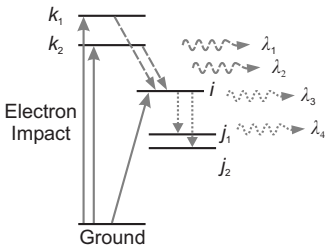

FIG. 3. Different ways of populating atomic levels after electron-impact excitation. Solid arrows show how electron impact directly excites the atom from the ground state and, consequently, populates levels k_1, k_2, and i. Level i, which decays to the lower levels j_1 and j_2 emitting light (dotted arrows), can also be populated by cascades from higher levels k_1 and k_2 (dashed arrows). Adapted from the website of the University of Wisconsin Atomic Collision Group (see Sec. V.C).

The electron beam is passed through the collision chamber filled with the gas of interest at a number density $\mathcal{N}$. The electron beam excites the gas atoms into many upper states, which will have a given probability for decaying to lower levels. Emissions from excited atoms are detected by means of an optical system. Absolute calibrations of the optical system are carried out by means of a standard tungsten lamp of known spectral irradiance. The wavelength for each transition is selected with the monochromator and detected with a photomultiplier tube (PMT).

The optical emission cross section Q_{ij}^{opt} for the transition $i \rightarrow j$ is the light intensity observed for one decay transition Φ_{ij} divided by the target number density and the electron beam flux,

$$Q_{ij}^{\mathrm{opt}} = \frac{\Phi_{ij}}{\mathcal{N} I/e}, \tag{29}$$

where I is the electron beam current and e is the charge of the electron. The sum of the optical emission cross sections for all transitions from i to the lower levels j is called the apparent excitation cross section,

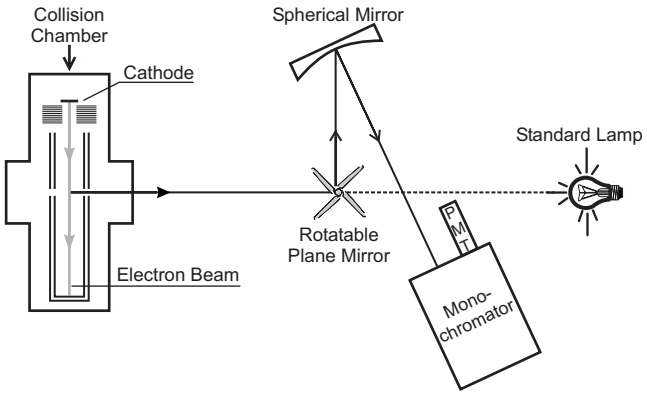

FIG. 4. Example of experimental setup for the measurement of excitation functions by means of optical methods. Adapted from the website of the University of Wisconsin Atomic Collision Group (see Sec. V.C).

$$Q_i^{\mathrm{app}} = \sum_{j<i} Q_{ij}^{\mathrm{opt}}. \tag{30}$$

As stated above, a level i may be populated both by direct electron-impact excitation and by higher excited levels k cascading into it. Therefore, the direct electron excitation cross section is obtained from the experimental data by subtracting from the apparent cross section the contribution of the cascades, which is the sum of the optical cross sections for transitions into level i from all the levels above it:

$$Q_i^{\mathrm{dir}} = Q_i^{\mathrm{app}} - \sum_{k>i} Q_{ki}^{\mathrm{opt}}. \tag{31}$$

The cascade transitions are often in the infrared region and are not readily detectable by a PMT. Solid-state devices, such as photodiodes, are sensitive to infrared emissions, but with the complication of a much lower signal-to-noise ratio than that of a PMT. A better signal-to-noise ratio can be obtained with a very long acquisition time for each spectral line. A Fourier-transform spectrometer overcomes this disadvantage by simultaneously observing all transitions within a broad spectral region (Chilton *et al.*, 1998).

B. Swarm techniques

The distinguishing feature of swarm experiments lies in the fact that they provide absolute electron cross sections for impact energies below 1 eV, accounting for scattering through all angles (Crompton, 1994; Inokuti *et al.*, 2000). These experiments, however, have the disadvantage of a complex analysis procedure to obtain cross-section data from transport coefficients, as discussed in the following.

While transport coefficients can be measured with relative uncertainties of about 1–2 % (Schmidt *et al.*, 1994), the solution of the Boltzmann equation [Eq. (18)] requires a number of approximations. One method consists in expanding $F(\vec{r},\vec{v},t)$ in terms of the electron density $n_e(\vec{r},t)$ and its spatial gradients, with expansion coefficients representing the electron velocity distribution functions (Pitchford *et al.*, 1981; Crompton, 1994),

$$F(\vec{r},\vec{v},t) = \sum_{k=0} f^k(\vec{v}) \otimes (-\vec{\nabla})^k n_e(\vec{r},t). \tag{32}$$

The velocity distribution functions $f^k(\vec{v})$ can be represented as spherical harmonic expansions and, if it can be assumed that the velocity dependence is isotropic, the harmonic expansion can be truncated after the second term (two-term approximation). This condition is met, for example, when performing swarm experiments with low-energy electrons in noble gases [for a review on this topic, see Pitchford *et al.* (1981) and Petrović *et al.* (1995)]. In this case, only elastic scattering occurs and the distribution function can be written as a function of the electron energy T as follows (Frost and Phelps, 1964):

$$f(T) = A \exp\left[- \int_0^T \left(\frac{M\mathcal{E}^2}{6m_e \mathcal{N}^2 \sigma_m^2(T) T} + \frac{k_B T_g}{e} \right)^{-1} dT \right], \tag{33}$$

where M is the atomic mass, $\mathcal{N}$ is the gas number density, $\mathcal{E}$ is the electric field strength, $\sigma_m(T)$ is the momentum transfer cross section of electrons of energy T, k_B is the Boltzmann constant, and T_g is the gas temperature. The constant A is defined such that $\int_0^\infty T^{1/2} f(T) dT = 1$. The drift velocity and the lateral diffusion coefficient can then be derived from the following equations:

$$v_d = - \frac{e\mathcal{E}}{3\mathcal{N}} \left(\frac{2}{m_e} \right)^{1/2} \int_0^\infty \frac{T}{\sigma_m(T)} \frac{d}{dT} f(T) dT, \tag{34}$$

$$D_T = \frac{1}{3\mathcal{N}} \left(\frac{2}{m_e} \right)^{1/2} \int_0^\infty \frac{T}{\sigma_m(T)} f(T) dT. \tag{35}$$

Equation (33) shows that, for swarm experiments performed in a noble gas under conditions of elastic scattering, the electron distribution function depends on the reduced electric field $\mathcal{E}/\mathcal{N}$. Moreover, at a given $\mathcal{E}/\mathcal{N}$ and T_g, the electron distribution function, and hence v_d and D_T, depends only on $\sigma_m(T)$. Provided there are no resonances or sharp maxima or minima in the momentum transfer cross section, $\sigma_m(T)$ can therefore be unfolded from experimental data for v_d and D_T as functions of $\mathcal{E}/\mathcal{N}$.

A major difficulty in determining scattering cross sections with a swarm technique is that the set of cross sections unfolded from Eqs. (34) and (35) is not unique because of uncertainties in measured transport coefficients and because of the increasing energy spread in the electron distribution function with increasing $\mathcal{E}/\mathcal{N}$. Moreover, for $\mathcal{E}/\mathcal{N} > 1$ Td,[1] the two-term approximation is not adequate for solving the Boltzmann equation; hence Eqs. (34) and (35) no longer apply (Petrović *et al.*, 1995). However, the choice of experimental conditions that ensure a small energy spread (low gas temperature) and elastic scattering only (low $\mathcal{E}/\mathcal{N}$ in noble gases) can reduce the number of possible cross sections [see Crompton (1994) for a detailed discussion of accuracy requirements for transport data].

In the case of elastic scattering only, generally at energies below 1 eV for noble gases, swarm-derived cross sections can be compared with those obtained in beam experiments. A direct comparison, however, is possible only for well-defined conditions: (i) at $T=0$ (experimentally unachievable), when the total and the momentum transfer cross sections are related to the scattering length A,

$$\sigma_{\text{tot}} = 4\pi A^2 = \sigma_{\text{el}} = \sigma_m, \tag{36}$$

and (ii) when the angular scattering is isotropic and $\sigma_{\text{tot}} = \sigma_m$. Given that, for argon, the angular scattering is not isotropic and a sharp Ramsauer-Townsend minimum characterizes the total cross sections at energies around 0.3 eV, a direct comparison between beam measurements and swarm-derived cross sections is not feasible; hence a theoretical approach must be used.

Several theoretical techniques that assist in this comparison have been developed in recent years, most based on a phase-shift analysis [for a comprehensive review, see Buckman and Brunger (1997)]. Using the well-known partial-wave expansion (Bransden and Joachain, 2003), the elastic, the momentum transfer, and the viscosity cross sections can be written, respectively, as follows:

$$\sigma_{\text{el}} = \frac{4\pi}{k^2} \sum_l (2l+1) \sin^2 \delta_l, \tag{37}$$

$$\sigma_m = \frac{4\pi}{k^2} \sum_l (l+1) \sin^2(\delta_l - \delta_{l+1}), \tag{38}$$

$$\sigma_v = \frac{4\pi}{k^2} \sum_l \frac{(l+1)(l+2)}{2l+3} \sin^2(\delta_{l+2} - \delta_l), \tag{39}$$

where δ_l is the phase shift at angular momentum l and k is the wave number. The use of a phase-shift analysis based on the modified effective range theory (MERT) allows parametrization of the energy dependence of scattering phase shifts in terms of dipole polarizability, effective range, and scattering length (O'Malley, 1963; Buckman and Mitroy, 1989). The advantages of this approach consist in (i) the possibility of extrapolating the cross sections to $T=0$, and (ii) the use of the same set of parameters to generate different types of cross sections. This implies that the parameters obtained to fit the momentum transfer cross section from a swarm experiment can be used to calculate the integrated elastic cross section according to Eq. (37) and then to compare the results with those obtained in a beam experiment. However, this technique can hardly be applied for energies above 1 eV, and care must be taken in the choice of the parametrization of phase shifts, as discussed by Buckman and Mitroy (1989).

When both elastic and inelastic scattering occur and the two-term approximation no longer applies, it is not possible to express the electron distribution function in a simple form like Eq. (33). Instead, the function has to be calculated by iteratively solving an integro-differential equation (see Puech and Torchin, 1986). Consequently, a unique set of cross sections cannot be determined from transport parameters, even if the experimental values have relative uncertainties of less than 1% (Crompton, 1994).

C. Photoabsorption and photoionization techniques

A variety of optically based methods are used for the determination of the optical oscillator strengths for discrete electronic transitions. An overview and a critical analysis of these methods was carried out by Gallagher

[1] 1 Townsend = 1 Td = 10^{-17} V cm^2.

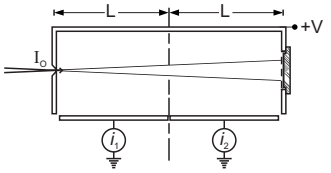

FIG. 5. Example of an experimental setup for measurements with a double ionization chamber. From Samson and Yin, 1989.

et al. (1988) and Chan *et al.* (1991). The measurement of the photoabsorption cross section σ_{abs} is based on the well-known Lambert-Beer law,

$$I = I_0 \exp(-\sigma_{abs}\mathcal{N}l). \tag{40}$$

Here I_0 and I are, respectively, the intensities of the radiation of energy $E_\nu = h\nu$ incident on and transmitted at a distance l through the absorbing gas, and $\mathcal{N}$ is the gas number density. Although this technique appears quite simple and easy to apply, some serious problems can affect the accuracy of the measurements. It should be noted, in fact, that Eq. (40) is valid only if the photon beam is perfectly monochromatic. This is not the case in a real experiment, in particular when dealing with synchrotron beamlines, where an optical monochromator is inserted between a continuum light source and the gas cell. The beam will therefore contain several energy components, depending on the energy resolution of the monochromator, and the absorption law will no longer consist of a single exponential function. This leads to an apparent dependence of the cross section on the thickness of the absorber. An effective method to reduce this effect is to carry out the experiments at different gas pressures (Chan *et al.*, 1991; Yang and Kirz, 1987). The sensitivity of the radiation detector to fluorescent light and to some instabilities in the intensity of the incident radiation gives rise to additional sources of uncertainty.

A device frequently used for photoabsorption measurements, which minimizes the effects described above, is the double ionization chamber (Samson and Yin, 1989; Sorokin *et al.*, 2000). It consists of a cylindrical absorption cell maintained at a positive potential with respect to two ion collectors of equal length L, as shown in Fig. 5. The photon radiation with initial intensity I_0 is absorbed exponentially and produces ions along its path. Provided that each electrode collects all ions directly above it, the total absorption cross section of the gas is given by

$$\sigma_{abs} = (1/\mathcal{N}L)\ln(i_1/i_2), \tag{41}$$

where i_1 and i_2 are currents flowing from the ion collectors. Some care should be taken in avoiding leakage currents between the absorption cell and the ion collectors, and pressure gradients within the vacuum housing of the double ion chamber. Sources of uncertainties can be significant in the measurement of gas pressure and electrode length as well as in the determination of the ion currents i_1 and i_2.

III. THEORETICAL BACKGROUND

As suggested by Bederson (1969), experimentalists should aim to perform "perfect scattering experiments," so that all aspects of a scattering process are determined at once. Similarly, theoreticians should provide a "complete scattering theory," which is able to describe not only "individual perfect scattering experiments for a particular scattering process, but also the possible scattering processes for a given incident projectile energy." This means that "a single calculation should yield accurate elastic, inelastic, excitation, and ionization scattering amplitudes" (Bray and Fursa, 1996).

The theoretical treatment of electron elastic and inelastic collisions has received a great deal of attention. For an overview of electron-atom and electron-ion scattering theories and appropriate calculation procedures, see Burke (1994), Schneider (1994), or the very recent work of Kallman and Palmeri (2007). Some concepts used for the analysis of the data are described in the following section.

A. General calculation methods

Quantum-mechanical approximations have been used to calculate elastic and inelastic cross sections with various degrees of success, but only for limited electron energy ranges. Approximations are made either in the description of the scattering potential or in the representation of the wave functions $\Psi(q_0, q_1, \ldots, q_N)$ that describe the projectile-target system according to Eq. (1).

The two commonly used approximations of the atomic potential are the Thomas-Fermi and Hartree-Fock potentials. The Thomas-Fermi model is based on statistical and semiclassical considerations and assumes that the N electrons of an atom form a Fermi gas in the ground state, confined to a region of space by a central potential $V(r)$. On the other hand, the Hartree-Fock, or self-consistent-field approximation, is more elaborate and assumes that electrons move in an effective potential that takes into account the attraction of the nucleus and the average effect of the repulsive interactions due to other electrons (Bransden and Joachain, 2003). A recent comparison that applies both approaches to the problem of solving the Dirac equation for electron elastic-scattering problems can be found in Jablonski *et al.* (2004).

The close-coupling (CC) method is the common way to approximate the wave functions by expanding them in terms that take into account all possible interaction channels of the system [for a general discussion about this method, see, for example, Schneider (1994)]. This method accurately describes a scattering process if it is applied while retaining all expansion terms, but, due to the huge number of equations (which tends to be infinite, in principle), this method converges very slowly. The simplest way of approximating the set of CC wave functions is to reduce it to one equation. The approximation to one equation is equivalent to an approximation of the wave function to the initial state of the target.

This is the so-called static-exchange approximation and applies to elastic collisions. In this case, the target atom is fully characterized by its nuclear and electronic charge distributions. Interaction with the incident particle is then described by (i) the electrostatic interaction with the atomic nucleus and the charge cloud of the target electrons, and (ii) the exchange force between electrons due to the Pauli exclusion principle.

The close-coupling description of elastic collisions works well for projectiles with energies above 5 keV. In fact, at intermediate energies (from 50 eV up to 5 keV), second-order effects, such as rearrangement collisions (in which the projectile exchanges place with an atomic electron), polarization of the target atom, and loss of flux from the elastic to the inelastic channels become important. They are taken into account by defining an optical potential as a sum of a static-exchange potential and other terms describing the mentioned second-order effects. Salvat (2003) calculated the differential and total elastic cross sections for electron and positron scattering by atoms and positive ions by using a semiempirical optical model potential instead of the static-exchange approximation, and found better agreement with the experimental data. The state of the art for this kind of calculation in the energy range 50 eV–5 MeV is the ELSEPA code, developed by Salvat *et al.* (2005).[2]

For elastic collisions at energies below 50 eV, the optical model also fails to give accurate results, because higher-order polarization effects, relativistic effects, and dynamic distortion effects play an increasing role. Some of these aspects has been discussed by Gibson *et al.* (1996) and Mielewska *et al.* (2004), who showed comparison between their experimental differential cross sections for argon (at energies between 1 and 10 eV) and several more complex theoretical models.

Khakoo *et al.* (2004) compared their measurements of the differential excitation cross sections for four argon configurations with several theoretical models, such as the widely used R-matrix method (Burke and Berrington, 1993) and the distorted-wave Born approximation (DWBA). The R-matrix method takes advantage of the fact that, for most collision problems, it is possible to partition the configuration space into an external and an internal region with respect to a sphere of well-defined radius $r=a$. This radius is chosen so that the charge distribution of the target states of interest is contained within the sphere. In the internal region of the configuration space ($r<a$), the interaction is strong, while in the external region ($r>a$) it is assumed that the projectile electron moves under the effect of an easily described potential. The DWBA makes use of the Born approximation and applies distortion factors to approximate the wave functions of both impinging and target electrons, describing the interaction either with the Thomas-Fermi or with the Hartree-Fock potential [see Bartlett and Stelbovics (2002), and references therein]. The work of Khakoo *et al.* showed that, despite the fact that many efforts have been made in recent years to improve the theoretical treatment of inelastic electron scattering with atoms, there is still disagreement between experimental and theoretical results, especially at energies below 50 eV.

Scaling methods were developed to determine electron-impact excitation cross sections on the basis of the Born approximation in order to account for electron exchanges with target electrons or target polarization. For example, the scaling method introduced by Kim (2001) is applicable to dipole-allowed excitations and requires knowledge of the binding energy of the electron being excited, the excitation energy, and an accurate oscillator strength for the transition.

Theoretical models based on empirical and semiempirical formulas or on classical and semiclassical collision theories have been developed since the 1920s. An extensive review of classical and semiclassical approximations for ionization cross sections was presented by Rudge (1968) and, more recently, by Kim and Rudd (1994) and Märk *et al.* (1995). One of the most general approaches for studying inelastic collisions—which is still under development—is the binary-encounter approximation [see Gryzinski and Kunc (2000), and references therein].

The peculiarity of this approximation is that two interacting particles are considered as a system of localized electrons and nuclei, described by a set of quantities such as the particle velocities, or the collision impact parameters. Therefore, a momentum or velocity distribution is also associated with the target particle. While application of the binary-encounter approximation for calculating excitation cross sections has not been widely explored up to now, several studies exist for ionization cross sections. The most successfully applied model is the so-called binary-encounter-Bethe (BEB) model (Kim and Rudd, 1994), which combines the binary-encounter cross section with the high-energy behavior of the Bethe-Born theory. The BEB ionization cross section for an atomic subshell i depends only on the orbital electron occupation number N_i, the orbital binding energy B_i, the kinetic energy T of the projectile electron, and the energy E of the ejected electron,

$$\sigma_{i,\mathrm{BEB}} = \frac{S_i}{t+u+1}\left[\frac{\ln t}{2}\left(1-\frac{1}{t^2}\right)+1-\frac{1}{t}-\frac{\ln t}{t+1}\right]. \quad (42)$$

Here $S_i=4\pi a_0^2 N_i (R/B_i)^2$, $t=T/B_i$, $u=U_i/B_i$, and $w=E/B_i$; U_i is the average orbital kinetic energy of the target electron.

This theory is free of adjustable or fitted parameters and can be easily extended to relativistic impact energies (Kim *et al.*, 2000).

The BEB theory for single-differential cross sections $d\sigma_i/dE$ depends also on the oscillator strength distribution,

[2]The program is available form the CPC Program Library, Queen's University of Belfast, N. Ireland, http://cpc.cs.qub.ac.uk/cpc/summaries/ADUS.

$$\frac{d\sigma_i}{dE} = \frac{d\sigma}{dw} = S_i \sum_{n=1}^{3} F_n(t)[f_n(w) + f_n(t-w)], \tag{43}$$

where

$$f_n(w) = (w+1)^{-n}, \quad f_n(t-w) = (t-w)^{-n}, \tag{44}$$

and

$$F_1 = -\frac{F_2(t)}{t+1}, \quad F_2 = \frac{2-Q}{t+u+1}, \quad F_3 = \frac{Q \ln t}{t+u+1} \tag{45}$$

with

$$Q = \frac{1}{N_i}\int_0^\infty (df/dw)dw. \tag{46}$$

Equation (43) assumes that the oscillator strength distribution df/dw is expanded in a power series in $(1+w)^{-n}$ starting from $n=2$ and that, for $w \gg 1$, only the first term of the expansion needs to be retained. However, if the oscillator strength distribution is not known, the further assumption $Q=1$ can be made.

Phenomenologically determined functions for interpolating the experimental data on excitation and ionization cross sections have also been suggested. In the following section, we give a brief account of the most used formulas, which are very useful for electron transport calculations.

B. Analytical formulas for inelastic cross sections

The analytical formula proposed by Green and Barth (1965) is useful to build a model for excitation cross sections,

$$\sigma_n(T) = \frac{q_0 G}{E_n^2}\left(1 - \frac{E_n}{T}\right)^{\nu}\left(\frac{E_n}{T}\right)^{1-\omega}, \tag{47}$$

where $q_0 = 4\pi a_0^2 R^2$, and G, ν, and ω are parameters to be adjusted. This phenomenological function, valid for both optically allowed and forbidden transitions, takes into account the general behavior of an excitation cross section, which starts to have nonzero values at threshold ($T=E_n$), rises according to some simple power law, and falls off following the Bethe-Born approximation. In Eq. (47), the term $[1-(E_n/T)]^{\nu}$ describes the threshold behavior and ω is related to the slope of the asymptotic cross section.

For optically allowed states, Paretzke (1989) defined an interpolation function that adds a distortion factor $\Psi(T)$ to the Bethe approximation function,

$$\sigma_n(T) = \Psi(T)\left[\frac{4\pi a_0^2 R}{T} M_n^2 \ln\left(\frac{4c_n T}{R}\right)\right], \tag{48}$$

where $\Psi(T) = 1 - \exp[-a(T/E_n - 1)]$ and a is a parameter to be adjusted. This distortion factor represents the low-energy behavior of the cross section (with threshold at $T=E_n$).

A simple formula for interpolating experimental total ionization cross sections was proposed by Kim and Rudd (1994),

$$\sigma_i(t) = \frac{4\pi a_0^2}{t}\left[a \ln t + b\left(1 - \frac{1}{t}\right) + c\frac{\ln t}{t+1}\right], \tag{49}$$

where a, b, and c are fitting parameters and $t = T/B_1$.

IV. CONSISTENCY REQUIREMENTS FOR CROSS-SECTION DATA

A. Primary requirements

The theoretical aspects of electron scattering by atoms discussed so far are well established, and will be used in this work to investigate the consistency of the collected data. In our analysis, we require (i) that the integrated cross sections obtained from Eq. (2) or (4) after extrapolating the missing data be in agreement with independent measurements of $\sigma(T)$, (ii) that the momentum transfer cross section obtained from Eq. (19) be in agreement with those obtained from Eq. (34) or (35), and (iii) that excitation and ionization cross sections vanish for energies below the threshold.

B. High-energy requirements

We require the validity of the Bethe theory for inelastic scattering of electrons at high energies [Eqs. (9), (11), and (13)]. For integrated excitation cross sections, we analyze the high-energy dependence by plotting the quantity $T\sigma_n/4\pi a_0^2 R$ against $\ln(T/R)$ (Fano, 1954).

We require the Fano plot to show (i) a straight line with slope $M_n^2 = f_n/(E_n/R)$ for optically allowed transitions [see Eq. (9)], and (ii) a constant for optically forbidden transitions [see Eq. (11)].

For ionization cross sections differential in energy, we require $d\sigma_i/dE$ to be proportional to the dipole oscillator strength distribution df/dE divided by E, as indicated by Eq. (13). We analyze this behavior by plotting the quantity

$$Y(E) = \frac{d\sigma_i}{dE}\frac{T}{4\pi a_0^2}\left(\frac{E}{R}\right)^2 \tag{50}$$

as a function of R/E (Platzman plot). Since for high impact energies the majority of secondary electrons are ejected in the low-energy range, we require $Y(E)$ for slow secondary electrons to be proportional to $E(df/dE)$ (Kim, 1975).

C. Optical data and sum rules requirements

The close connection between high-energy electron scattering and photoabsorption provides useful relationships for data consistency checks in the limit $K \to 0$ of the generalized oscillator strength distribution.

The μth moment of the oscillator strength distribution is defined as follows:

$$S(\mu) = \sum_n (E_n/R)^\mu f_n + \int_{B_1}^{\infty} (E/R)^\mu (df/dE) dE \equiv \sum\!\!\!\!\!\!\int_n (E_n/R)^\mu f_n. \quad (51)$$

Some of the moments can be expressed in terms of simple formulas and are related to optical properties of matter, such as, for example, the refractive index or the polarizability (Fano and Cooper, 1968; Eggarter, 1975). The zeroth moment is the Thomas-Reiche-Kuhn sum rule for an atom containing Z electrons,

$$S(0) = \sum\!\!\!\!\!\!\int_n f_n = Z. \quad (52)$$

For $\mu=-1$, Eq. (51) yields

$$S(-1) = \sum\!\!\!\!\!\!\int_n (R/E_n) f_n = \sum\!\!\!\!\!\!\int_n M_n^2 = M_{\text{tot}}^2. \quad (53)$$

M_{tot}^2 represents the sum of the dipole matrix element squared, defined by Eqs. (8) and (15).

The refractive index n_ν is related to the oscillator strength via the following relationship:

$$n_\nu = 1 + 8\pi \mathcal{N} a_0^3 R^2 \sum\!\!\!\!\!\!\int_n [f_n/(E_n^2 - E_\nu^2)], \quad (54)$$

where $\mathcal{N}$ is the atomic number density and $E_\nu = h\nu$ is the energy of the incident radiation. If E_ν^2 is smaller than E_n^2 for all states, we can expand Eq. (54) in powers of $(E_\nu/E_n)^2$ and obtain a series whose coefficients are the negative even moments of the oscillator strength distribution,

$$n_\nu = 1 + 8\pi \mathcal{N} a_0^3 \sum_{\mu=1}^{\infty}\!\!\!\!\!\!\int S(-2\mu)(E_\nu/R)^{2\mu-2}. \quad (55)$$

Another optical quantity that can be expressed in terms of moments of the oscillator strength distribution is the Verdet constant V_ν, defined as

$$V_\nu = \frac{1}{H}\frac{d\Theta}{dz} = \frac{eR^2}{m_e c^2} 8\pi \mathcal{N} a_0^3 E_\nu^2 \sum\!\!\!\!\!\!\int_n \frac{f_n}{(E_n^2 - E_\nu^2)^2}, \quad (56)$$

where $d\Theta/dz$ is the rotation of the polarization plane per unit path length experienced by a beam of polarized light traversing a dispersive medium in the presence of an axial magnetic field of strength H. The sum in Eq. (56) can also be expanded as follows:

$$V_\nu = \frac{e}{m_e c^2} 8\pi \mathcal{N} a_0^3 \left(\frac{E_\nu}{R}\right)^2 \sum_{\mu=1}^{\infty}\!\!\!\!\!\!\int S(-2\mu)\left(\frac{E_\nu}{R}\right)^{2(\mu-2)}. \quad (57)$$

In addition, the second negative moment is related to the electric dipole polarizability at zero frequency,

$$\alpha(0) = (e^2\hbar^2/m_e R^2) S(-2) = 4\pi\epsilon_0 a_0^3 S(-2), \quad (58)$$

where ϵ_0 is the vacuum permittivity.

We take Eqs. (52), (53), (55), (57), and (58) as decisive constraints for testing the normalization and consistency of the optical oscillator strengths.

TABLE I. Most relevant experimental work on optical oscillator strengths for argon of the last 30 years.

Author	Technique	Type of data
Suzuki and Saito, 2005	PI[a]	df/dE
Stewart *et al.*, 2002	OEM[b]	f_n
Sorokin *et al.*, 2000	PI	df/dE
Tsurubuchi *et al.*, 1996	OEM	f_n
Wu *et al.*, 1995	EELS[c]	f_n
Gibson and Risley, 1995	SA[d]	f_n
Chan *et al.*, 1992	EELS	df/dE, f_n
Samson and Yin, 1989	PA[e]	df/dE
Li *et al.*, 1988	EELS	f_n
Yang and Kirz, 1987	PA	df/dE
Chornay *et al.*, 1984	LT[f]	f_n
Westerveld *et al.*, 1979	SA	f_n
Vallee *et al.*, 1977	LB[g]	f_n
Copley and Camm, 1974	LB	f_n
Irwin *et al.*, 1973	LT	f_n
McConkey and Donaldson, 1973	OEM	f_n

[a]Photoionization measurements.
[b]Optical emission measurements.
[c]Electron energy-loss spectroscopy.
[d]Self-absorption.
[e]Photoabsorption measurements.
[f]Lifetime measurements.
[g]Measurements of line broadening.

V. DATA ANALYSIS

We begin with the treatment of the optical oscillator strengths (OOSs) because these data are used afterward to test the inelastic electron cross sections at high impact energies.

We report in Table IX (Appendix A) the argon energy levels, whose excitation cross sections and optical data are main focus of this work. In Table X (Appendix A), we list binding energies (B_i), kinetic energies (U_i), and orbital occupation numbers (N_i) of Ar.

A. Optical oscillator strengths

The OOSs reported for argon in the past three decades were derived using various techniques (see Table I and the review of Berkowitz, 2002). Extensive measurements were carried out by Chan *et al.* (1992) using a high-resolution dipole electron-scattering spectrometer in the limit of zero-degree scattering angle (i.e., negligible momentum transfer, which corresponds to the optical limit). Chan *et al.* obtained absolute values for the discrete, continuum, and autoionizing regions, up to an energy loss of 500 eV. Several others were concerned with measurements of the photoabsorption cross section in the continuum region. For these data, we calculated the OOS values by means of Eq. (17).

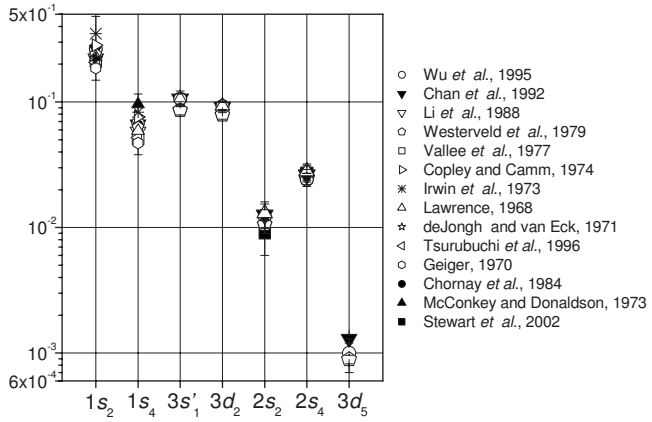

FIG. 6. Schematic diagram of discrete optical oscillator strengths f_n (ordinate axis) for transitions from the ground state of the argon atom (indicated on the abscissa in Paschen notation).

1. Discrete transitions

The optical oscillator strengths for the state[3] $1s_2$ show significant discrepancies, up to about 40%, mostly between values obtained with different experimental techniques (see Table XI in Appendix B and, for a qualitative presentation, Fig. 6). If we consider only the data resulting from energy-loss spectroscopy, or only those from optical emission measurements, the maximum difference reduces to approximately 22%. Nevertheless, the exclusion of very discrepant data [such as, for example, those of Irwin *et al.* (1973)] would modify the weighted mean by less than 1%. The discrepancies for the state $1s_4$ range from 2% to about 47%, and can differ by about 35% even if measured with the same technique. Also in this case the exclusion of some data (such as, for instance, the value obtained by McConkey and Donaldson, 1973) would affect the weighted mean by less than 1%. For states from $3s_1'$ to $3d_5$, the few data available are typically in agreement to within 20%.

For higher-energy states, the data are scarce, reflecting the difficulties in measuring cross sections and optical data when the energy difference between adjacent levels is too small (Chan *et al.*, 1992; Weber *et al.*, 2003).

We created a set of f_n values for discrete states by calculating a weighted mean of all data available for states from ground up to the states of configuration $3p^5 5s$, and by using the results for some transitions to higher discrete states provided by Chan *et al.* Our compilation (see Table XI) is in good agreement with the data adopted by Eggarter (1975) and Berkowitz (2002) and those listed in the NIST database. The total discrete OOSs up to the ionization threshold determined by Chan *et al.* (1992) and reported by Berkowitz are in agreement to within 8% with that given by Eggarter. The sum of our adopted f_n values for the resolved states included in Table XI is 0.723 ± 0.014, which is about 16% lower than the total discrete OOS given by Chan *et al.* or by Berkowitz. As stated above, this is due to the lack of resolved OOS data for higher atomic levels.

[3]In this work, we use the Paschen notation to denote the discrete energy levels.

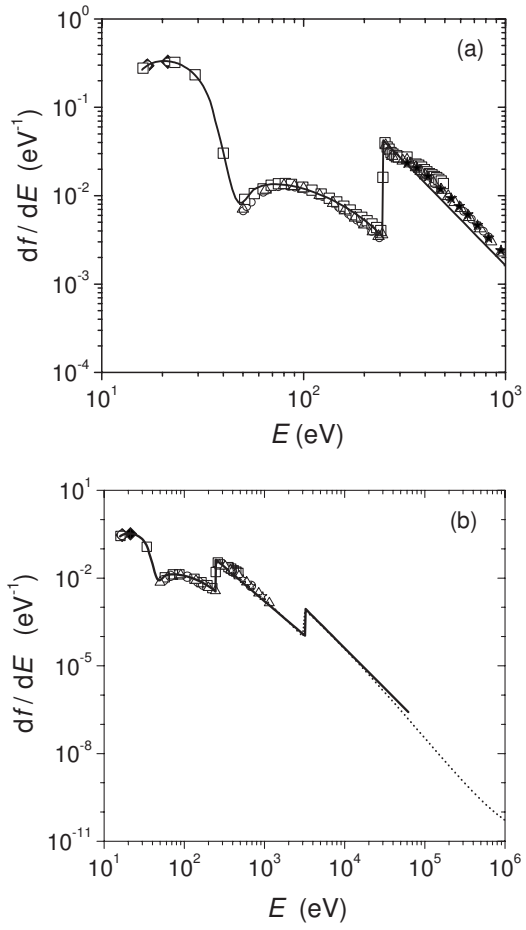

FIG. 7. Optical oscillator strength distributions in the energy range (a) 10–1000 eV and (b) 10 eV–1 MeV. Solid line, Marr and West (1976); dashed line, NIST XCOM database (Berger *et al.*, 2005); experimental data: ★, Yang and Kirz (1987); ♦, Samson and Yin (1989); ○, Sorokin *et al.* (2000); △, Suzuki and Saito (2005); □, Chan *et al.* (1992). The data recommended by Henke *et al.* (1993) and Berkowitz (2002) are not shown for clarity.

2. Continuum region

Compilations of photoionization and photoabsorption cross sections for Ar were presented by Marr and West (1976), Henke *et al.* (1993), Cooper (2000), Sorokin *et al.* (2000), and Berkowitz (2002). Marr and West reviewed existing experiments and built a recommended set using polynomial fits. The best-fit values of the photoabsorption cross sections reviewed by Henke *et al.* were obtained using the relativistic calculations of Doolen and Liberman (1987). The cross sections reported by Sorokin *et al.* consist in a selection of measurements performed after 1960 with relative uncertainties of less than 7%. The analysis made by Berkowitz is very detailed and provides best-fit values to four-term polynomials. The mentioned compilations are consistent (within 15%), for energies below 350 eV (see Fig. 7). At higher energies,

the values in Sorokin *et al.* and Henke *et al.* are higher than those in Marr and West by approximately 20–35 %. New photoabsorption measurements were published by Suzuki and Saito (2005) in the energy range 50–1150 eV. These data and those of Samson and Yin (1989), obtained at low photon energies, are in good agreement with the compilations of Henke *et al.* and Sorokin *et al.* Yang and Kirz (1987) measured the photoabsorption cross section in the range from about 320 up to 950 eV. The resulting OOS distribution is systematically higher than that of Marr and West, but in good agreement (within 5–8 %) with that of Henke *et al.* The NIST XCOM database (Berger *et al.*, 2005) provides photoabsorption cross sections for energies in the range 1 keV–100 GeV. The agreement of the NIST data with those of Marr and West and Henke *et al.* is between 5% and 25%, apart from the value at the *K*-absorption edge ($E=3203$ eV), where the difference between the NIST value and that reported by Marr and West is almost a factor of 8. This difference is due, among in part other reasons, to the energy resolution limit of four significant digits in the XCOM calculations, which can affect the location of the edge. For energies below 200 eV, data tabulated in the NIST FFAST database (Chantler *et al.*, 2005) are expected to have uncertainties between 50% and 100%; thus they are excluded from this analysis [see Chantler *et al.* (2005), and references therein for more details]. A comparison with the results obtained by Chan *et al.* (1992) shows again, as can be seen in Fig. 7, that the compilation of Marr and West is systematically too low for values above 350 eV. Clearly, more experiments are necessary, especially at energies above 1 keV, where the old data are not reliable. We built a complete oscillator strength distribution by adopting the data of Marr and West between threshold and about 40 eV and by calculating weighted average values between 40 eV and 1 keV. Between 1 and 100 keV, we normalized the data of Marr and West to those of Suzuki and Saito using a factor of 1.28. This factor was calculated using the mean value of the ratio of the two data sets between 440 and 1100 eV. Above this energy, we adopted the NIST data.

3. Sum rules

We chose to use the sum rules (see Sec. IV.C) as the main criteria for verifying the consistency of the discrete and continuum optical oscillation strengths and the total ionization cross section. Equation (51) was solved for $\mu=0$, -1, and -2. The value $S(0)=18.643$ differs from $Z=18$ by approximately 3.6%, compatible with the overall uncertainty on $S(0)$. Berkowitz (2002) obtained $S(0)=17.885$. Our values $S(-1)=4.330$ and $S(-2)=2.673$ are in good agreement with the corresponding values reported by Berkowitz [$S(-1)=4.3331$ and $S(-2)=2.7305$].

Comparisons with some literature data on the refractive index, the electric dipole polarizability, and the Verdet constant are summarized in Table II. The agreement confirms the validity of the normalization that we applied to the data of Marr and West.

TABLE II. Argon optical data used for consistency checks. The dependence on frequency is expressed through the wavelength $\lambda=c/\nu$.

Wavelength λ (nm)	Property	Equation	This work	Other work
400	$10^6\times(n_\nu-1)$	(54)	276.52	
700			270.47	
1.25×10^7			267.67	277.8[a]
0	$\alpha(0)$	(58)	10.691 a.u.[b]	11.074 a.u.[c] 10.175 a.u.[d]
400	V_ν	(57)	0.744 a.u.[e]	0.7245 a.u.[c]
700			0.229 a.u.	0.2222 a.u.[c]
850			0.154 a.u.	0.1493 a.u.[c]

[a] Kaveeshwar *et al.* (1976).
[b] 1 a.u. $=e^2a_0^2R^{-1}=4\pi\epsilon_0a_0^3=1.648\,78\times10^{-41}$ C^2 s^{-2} kg^{-1}.
[c] See Jasuński *et al.* (1995) for a summary of calculated and experimental results.
[d] Froome (1955).
[e] 1 a.u. = rad $ea_0\hbar=8.039\,624\times10^4$ rad T^{-1} m^{-1}.

B. Elastic cross sections

Argon elastic differential cross sections have been measured extensively since the 1930s, typically for impact energies between a few and 100 eV (see Table III). Measurements of elastic differential cross sections are usually limited to a scattering angle range between about 20° and 130°. Only recently, with the development of the magnetic angle-changing technique, has the full angular range of backward scattering become available (Zubek *et al.*, 1996). The shape of the differential cross section and the position of minima play an important role in comparing experimental data with theoretical models and in the determination of the integrated cross sections.

Among the available experimental data, summarized in Table III, we selected only the differential cross sections for which the integral could be calculated using Eq. (2). For this reason, measurements performed in a small angular range were not considered. Williams and Willis (1975), Hyder *et al.* (1986), and Cvejanović and Crowe (1997) reported only differential cross sections. Therefore, we fitted their data using an analytical function.

Sources of uncertainties for the measured differential cross sections include (i) the angular spread of the electron beam, (ii) fluctuations in size and electron density of the beam, (iii) changes in the transmission efficiency of the spectrometer, and (iv) the finite angular resolution of the analyzer [as can be deduced from Eq. (21)]. Background scattering, fluctuations in pressure, and primary-electron current also play a significant role. Moreover, the spin polarization of scattered electrons has a maximum in the vicinity of the cross-section minima and changes dramatically within a very small angular range. Thus a polarization analysis of scattered electrons should be conducted when measuring differential cross sections.

TABLE III. Summary of available electron elastic differential cross sections for argon. If not stated otherwise, the measurements were performed using a crossed-beam technique.

Author	Type of measurement	Energy range (eV)
Mielewska *et al.*, 2004	Relative[a]	5–10[b]
Panajotović *et al.*, 1997	Relative[c]	10–100
Cvejanović and Crowe, 1997	Relative[c]	20.43–110
Gibson *et al.*, 1996	Relative-flow technique[a]	1–10
Furst *et al.*, 1989	Relative-flow technique[a]	3–20
Weyhreter *et al.*, 1988	Relative-flow technique[a]	0.05–2
Iga *et al.*, 1987	Relative-flow technique[d]	300–1000
Hyder *et al.*, 1986	Relative[c]	100–300
Williams and Willis, 1975	Absolute	20–400
Srivastava *et al.*, 1981	Relative-flow technique[a]	3–100
Jansen *et al.*, 1976[e]	Relative[d]	100–3000[f]
DuBois and Rudd, 1976[e]	Absolute	20–800
Vušković and Kurepa, 1976[e]	Absolute	60–150

[a]Relative to He.
[b]Angular range 130°–180°.
[c]Normalized to prior work.
[d]Relative to N_2.
[e]Use of a static-target technique.
[f]Angular range 5°–55°.

For cross sections obtained with a normalization procedure or with the relative-flow technique, the accuracy of the reference data must be carefully verified. Finally, the uncertainty due to the data-fitting procedure must be taken into account in calculating the total uncertainty of the integrated cross sections.

As an example, Fig. 8 shows the differential cross sections for elastic scattering at $T=10$ eV. The magnetic angle-changing technique leads to accurate results in the backward-scattering angular range, hence highlighting the discrepancies among results obtained with different theoretical treatments of elastic scattering at low energies. We point out again that relativistic effects and target polarization play an important role at low electron impact energies; therefore, they should not be neglected in theoretical models. The relativistic calculations performed by Nahar and Wadehra (1991) to determine low-energy elastic and momentum transfer cross sections showed, in fact, that the differences with respect to the

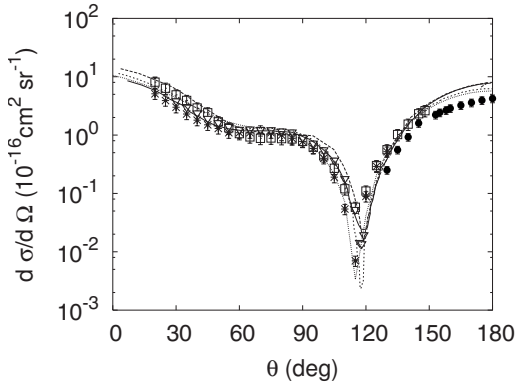

FIG. 8. Differential elastic cross sections for an electron-impact energy $T=10$ eV. Experimental data: *, Srivastava *et al.* (1981); □, Panajotović *et al.* (1997); ●, Mielewska *et al.* (2004); ▽, Gibson *et al.* (1996). Phase-shift analysis: solid line, Gibson *et al.* (1996). Theoretical models as follows. Dashed line, Bell *et al.* (1984). This calculation is based on an *R*-matrix theory and does not take into account spin-orbit coupling. Short dashed line, McEachran and Stauffer (1997). This relativistic treatment takes into account polarization and dynamic distortion effects. dotted line, Nahar and Wadehra (1987). This nonrelativistic treatment takes into account the target polarization, but does not consider spin-orbit effects.

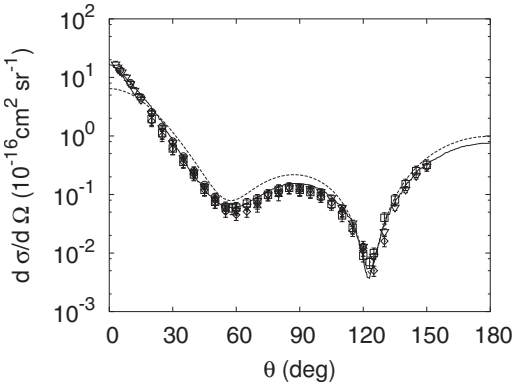

FIG. 9. Differential elastic cross sections for an electron-impact energy $T=100$ eV. Experimental data: □, Panajotović *et al.* (1997); ◇, Srivastava *et al.* (1981); ○, Jansen *et al.* (1976); ▽, DuBois and Rudd (1976); △, Cvejanović and Crowe (1997). Calculations: dashed line, NIST database (Jablonski *et al.* 2002); solid line, Salvat (2003).

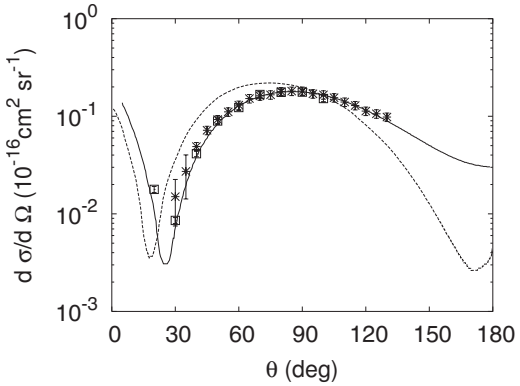

FIG. 10. Differential elastic cross sections for an electron-impact energy $T=1$ eV. Experimental data: □, Weyhreter *et al.* (1988); *, Gibson *et al.* (1996); dashed line, Haddad and O'Malley (1982). Calculations: solid line, McEachran and Stauffer (1997).

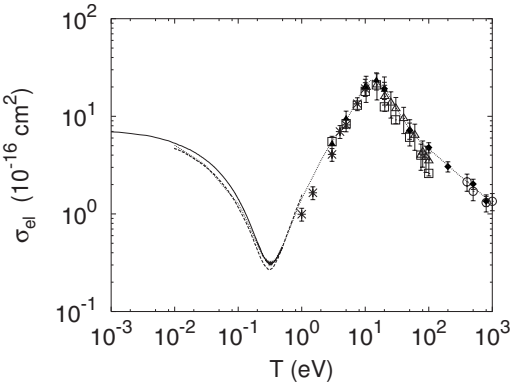

FIG. 11. Integrated elastic cross sections for Ar. Experimental results: *, Gibson *et al.* (1996); △, Panajotović *et al.* (1997); ○, Iga *et al.* (1987); □, Srivastava *et al.* (1981); ♦, DuBois and Rudd (1976); ▲, Furst *et al.* (1989); solid line: Weyhreter *et al.* (1988); dashed line: Haddad and O'Malley (1982). The data adopted by Hayashi (2003) are also shown for comparison (dotted line).

nonrelativistic calculation are about 30% at 3 eV, but decreased with increasing energy (about 1.5% at 300 eV). The example at $T=10$ eV also shows that the data extrapolation procedure for θ close to 180°, by using phase-shift analysis, can overestimate measured cross-section values by as much as 55% [see Mielewska *et al.* (2004), and references therein].

In Fig. 9, we present a comparison between experimental and calculated data for the differential cross section at $T=100$ eV. The calculated NIST cross sections are based on a solution of the Dirac equation with the static-exchange approximation (Jablonski *et al.*, 2002). The introduction of an optical potential, taking into account both target polarization and losses of flux from the elastic channel to inelastic channels, further improves the already satisfactory agreement with experimental results (Salvat, 2003).

As mentioned in Sec. II.B, elastic cross sections can also be determined from swarm experiments using the MERT. Figure 10 shows the differential cross section at $T=1$ eV determined from different types of experiments. The agreement between data obtained from beam experiments is within the overall uncertainty, while the data of Haddad and O'Malley (1982), from a MERT evaluation, show (i) a shift in the position of the minima and (ii) discrepancies that reach almost a factor of 4 in the backward-scattering region. Since the relativistic calculations of McEachran and Stauffer (1997) well reproduce the experimental cross sections of Weyhreter *et al.* (1988) and Gibson *et al.* (1996), it is possible that the upper energy limit for applying the MERT, indicated by Haddad and O'Malley as 1 eV, is too high or that the chosen parametrization for the phase shifts is not appropriate [as indicated by Buckman and Mitroy (1989) for integrated elastic cross sections].

Figure 11 shows the various integrated elastic cross sections as a function of the electron-impact energy. There is agreement within less than 20% at very low and

TABLE IV. Summary of available electron momentum transfer cross sections for argon.

Author	Type of measurement	Type of data	Energy range (eV)
Mielewska *et al.*, 2004	EB[a]	σ_m	5–10[b]
Panajotović *et al.*, 1997	EB	σ_m, σ_v	10–100[b]
Gibson *et al.*, 1996	EB	σ_m	1–10[b]
Suzuki *et al.*, 1990	SA[c]	σ_m	0.02–100
Schmidt *et al.*, 1994	SA	σ_m	0.007–3
Nakamura and Kurachi, 1988	SA	σ_m	2.5–15
Weyhreter *et al.*, 1988	EB	σ_m	0.05–2
Žigman and Milić, 1988	SA	σ_v	0.13–15
Haddad and O'Malley, 1982	SA	σ_m	0.01–10
Srivastava *et al.*, 1981	EB	σ_m	3–100[b]
Frost and Phelps, 1964	SA	σ_m	0.002–20

[a]Electron beam.
[b]See Table III for details.
[c]Swarm analysis.

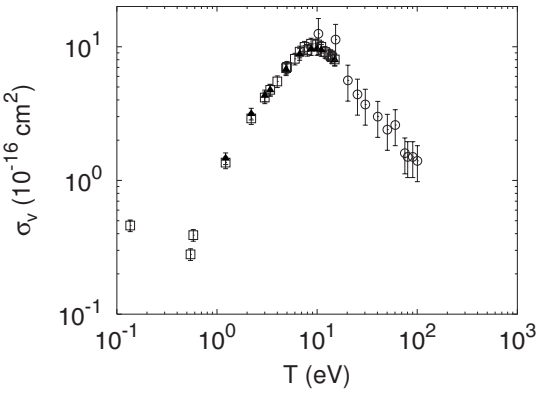

FIG. 12. Viscosity cross sections for Ar. Results from beam experiments: ○, Panajotović *et al.* (1997); results from a MERT analysis of phase shifts: □, Žigman and Milić (1988) with phase shifts from McEachran and Stauffer (1983); ▲, Žigman and Milić (1988) with phase shifts from Williams (1979).

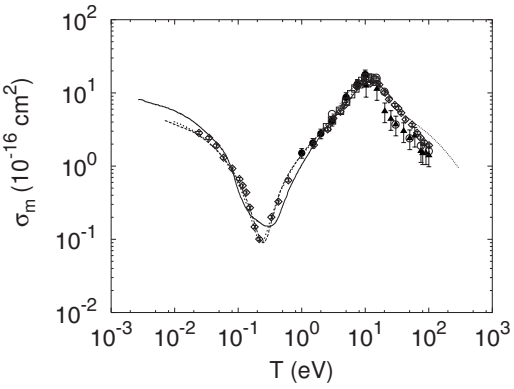

FIG. 13. Momentum transfer cross sections for Ar. Results from beam experiments: ●, Gibson *et al.* (1996); ▲, Panajotović *et al.* (1997); ○, Srivastava *et al.* (1981). Results from swarm experiments: long dashed line, Schmidt *et al.* (1994); solid line, Frost and Phelps (1964); □, Nakamura and Kurachi (1988); ◇, Suzuki *et al.* (1990). Theoretical results: short dashed line, McEachran and Stauffer (1997); dotted line, Nahar and Wadehra (1987).

high energies, and within 30% at intermediate energies, compatible with the stated overall uncertainties. In view of this fact, we compiled a new set of data by calculating a weighted mean of the selected experimental cross sections.

1. Momentum transfer and viscosity cross sections

In Table IV, we summarize relevant data on momentum transfer and viscosity cross sections for elastic scattering. Unfortunately, experimental viscosity cross sections (shown in Fig. 12) were reported only by Žigman and Milić (1988) and Panajotović *et al.* (1997). Žigman and Milić evaluated σ_v from two different phase-shift data using Eq. (39), while Panajotović *et al.* (1997) integrated the measured elastic differential cross sections using Eq. (20). Agreement for $T=10$ and 15 eV, where independent measurements are available, is within 30%.

Figure 13 shows a selection of momentum transfer cross sections obtained with beam measurements and swarm analysis. Agreement, in the energy range where both methods are applicable, is within 30%, compatible with the overall uncertainties. The theoretical calculations of Nahar and Wadehra (1987) (who solved the Schrödinger equation using a semiempirical polarization potential) and McEachran and Stauffer (1997) (who solved the Dirac equation taking into account spin-polarization and dynamic distortion effects) are also in good agreement with experiments.

We adopted a set of momentum transfer cross sections based on the weighted mean of recent experimental data.

TABLE V. Summary of available electron excitation cross sections for argon.

Author	Levels[a]	Impact energy T (eV)
Khakoo *et al.*, 2004[b]	$1s_2-1s_5$	$14\leqslant T\leqslant 100$
Stewart *et al.*, 2002[c]	$2s_2,2s_4,3d_5$	$E_n\leqslant T\leqslant 200$
Filipović *et al.*, 2000a[b]	$1s_2,2p_1,2p_{10}$	$16\leqslant T\leqslant 80$
Filipović *et al.*, 2000b[b]	$1s_3,1s_4,1s_5$	$20\leqslant T\leqslant 80$
Chilton and Lin, 1999[c]	$3p^5 3d,3p^5 5s$	$E_n\leqslant T\leqslant 200$
Chilton *et al.*, 1998	$2p_1-2p_{10}$	$E_n\leqslant T\leqslant 300$
Tsurubuchi *et al.*, 1996[c]	$1s_2,1s_4$	$E_n\leqslant T\leqslant 1000$
Schappe *et al.*, 1994[c]	$1s_3,1s_5$	$E_n\leqslant T\leqslant 100$
Ajello *et al.*, 1990	$1s_2,1s_4$	200[d]
Li *et al.*, 1988[b]	$1s_2,1s_4$	400,500
Chutjian and Cartwright, 1981[b]	$3p^5 4s,3p^5 4p,3p^5 3d$	$16\leqslant T\leqslant 100$
McConkey and Donaldson, 1973[c]	$1s_2,1s_4$	$10\leqslant T\leqslant 2000$[d]

[a]See Table IX for level notation and energy.
[b]Electron energy-loss spectroscopy.
[c]Optical emission measurements.
[d]Apparent cross section; see text.

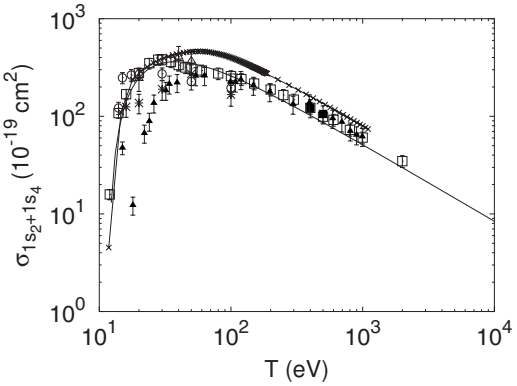

FIG. 14. Sum cross section for levels $1s_2$ and $1s_4$. Experimental data: □, Ajello *et al.* (1990); ○, Khakoo *et al.* (2004); ■, Li *et al.* (1988); ▲, Tsurubuchi *et al.* (1996); △, Filipović *et al.* (2000a); *, Chutjian and Cartwright (1981). Compilations: solid line, this work; (–×–), Eggarter (1975).

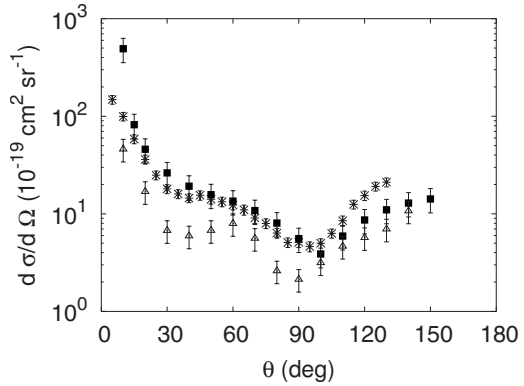

FIG. 15. Differential cross sections for the level $1s_2$ at T =20 eV. *, Khakoo *et al.* (2004); ■, Filipović *et al.* (2000a); △, Chutjian and Cartwright (1981).

C. Excitation cross sections

Electron excitation cross sections for Ar have been measured for a few atomic levels only and for limited impact energy ranges. In the past 15 years, several groups have started systematic studies for impact energies up to 100–200 eV (see Table V). The Atomic Collision group at the University of Wisconsin (Schappe *et al.*, 1994; Chilton *et al.*, 1998; Piech *et al.*, 1998; Boffard *et al.*, 1999; Chilton and Lin, 1999; Stewart *et al.*, 2002; Weber *et al.*, 2003) is involved in the collection of data using optical techniques for transitions of several excited states out of the ground level and out of metastable levels. Some tabulated data are available on the website: http://raptor.physics.wisc.edu. Boffard *et al.* (2004) reviewed excitation cross sections for noble gases for applications in plasma diagnostics, and Yanguas-Gil *et al.* (2005) compiled a coherent set of argon inelastic cross sections for applications in plasma discharge modeling, checking the data consistency by solving the two-term Boltzmann equation for a direct-current argon plasma. Following the first comprehensive study of Chutjian and Cartwright (1981), progress has been made in the measurement of differential cross sections by means of electron energy-loss spectroscopy (Filipović *et al.*, 2000a, 2000b; Khakoo *et al.*, 2004). The pioneering work of Eggarter (1975) was based on a relatively poor collection of experimental data; therefore the shape of the cross sections was derived from several theoretical assumptions that had to satisfy a number of consistency constraints.

1. Optically allowed states

Differences between the cross sections for resonance states $1s_2$ and $1s_4$ can be remarkable for energies between threshold and 50 eV, as we report in Fig. 14. Chutjian and Cartwright (1981), Filipović *et al.* (2000a), and Khakoo *et al.* (2004) determined the differential cross sections for these states with electron energy-loss spectroscopy using the relative-flow technique and normalized their data to the elastic cross sections for Ar. The discrepancy in the absolute values can amount to up to 70%. In these works, the inelastic energy-loss spectrum was measured for each impact energy and scattering angle of interest. The peak intensity of the $1s_2$ state was then normalized to the elastic peak intensity and scaled to absolute values using experimental cross sections from the literature. The peak intensity of the $1s_4$ state was normalized to the $1s_2$ peak intensity. This procedure is sensitive to the placement of the analyzer, which can affect the measurement reproducibility around the cross-section minima (see Khakoo *et al.* for

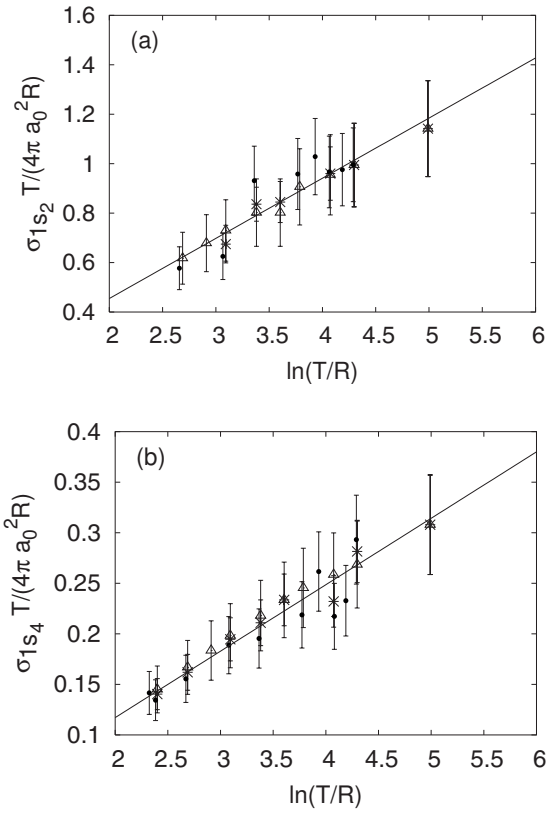

FIG. 16. Fano plot for the levels (a) $1s_2$ and (b) $1s_4$. △, Ajello *et al.* (1990); ●, Tsurubuchi *et al.* (1996); *, new compilation. Solid line, linear fit to the new compiled data.

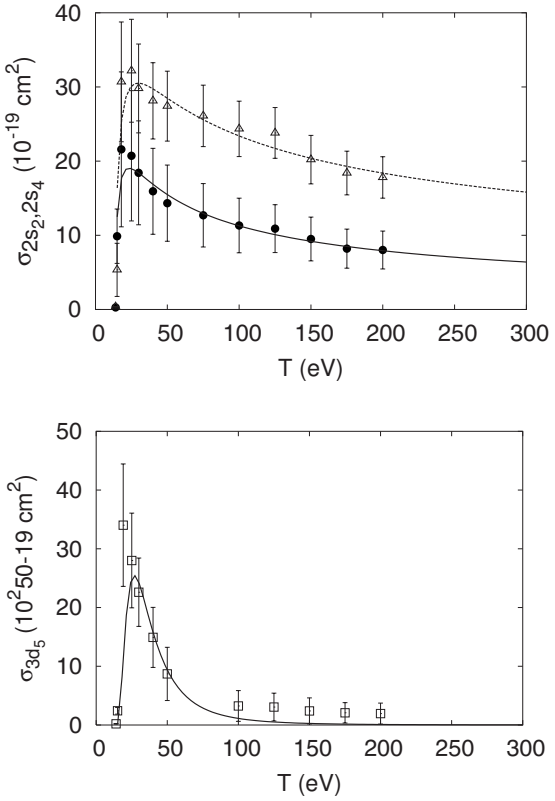

FIG. 17. Excitation cross sections for the states $2s_2$ (△), $2s_4$ (●), and $3d_5$ (□). The lines represent the respective interpolation functions obtained using Eq. (47).

discussion). Moreover, the accuracy of the transmission efficiency η of the apparatus [Eq. (21)] can be influenced by the method used to measure the inelastic-to-elastic intensity ratio. In particular, the focusing characteristics of the spectrometer should be carefully optimized (Filipović *et al.*, 2000a).

It should also be pointed out that the three sets of differential cross sections obtained via electron energy-loss spectroscopy show discrepancies of up to a factor of 3 at low energies (see Fig. 15). This might be due to the different normalization data adopted to scale the

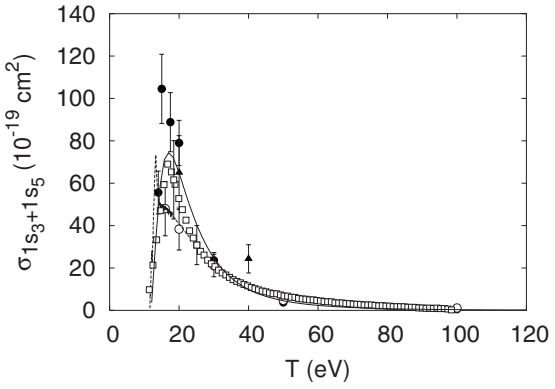

FIG. 18. Sum cross sections for levels $1s_3$ and $1s_5$. Experimental data: ●, Khakoo *et al.* (2004); ▲, Filipović *et al.* (2000b); ○, Chutjian and Cartwright (1981); □, Schappe *et al.* (1994). Compilations: solid line, this work; dashed line, Eggarter (1975).

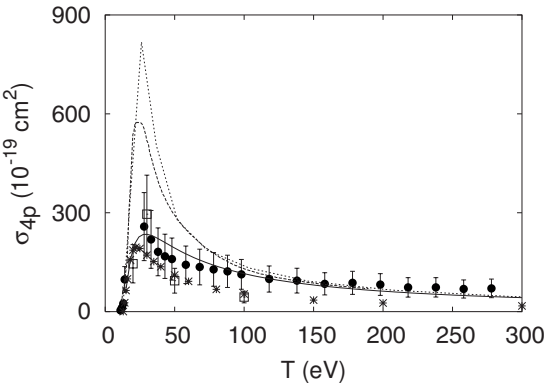

FIG. 19. Sum cross sections for $4p$ levels. Experimental results: ●, Chilton *et al.* (1998); □, Chutjian and Cartwright (1981). Compilations: solid line, this work; dashed line, Eggarter (1975); dotted line, IAEA database; *, Hayashi (2003).

relative-flow measurements into absolute values (Khakoo *et al.*, 2004). The agreement, however, improves at energies above 50 eV.

Problems also arise if optical methods are used. Tsurubuchi *et al.* (1996) measured both the relative excitation function and the cascade contribution to the $1s_2$ and $1s_4$ levels. They normalized the excitation functions by combining the direct cross sections of Li *et al.* (1988) at $T=500$ eV and their own value for the cascade contributions at the same energy. Consequently, they obtained the direct cross sections by subtracting the cascade contribution from the excitation functions. Ajello *et al.* (1990) measured the apparent cross sections at 200 eV and used the energy dependence of the excitation functions measured by McConkey and Donaldson (1973), but after having to renormalize them. In fact, McConkey and Donaldson erroneously assumed very small or no cascading contributions to the excitation functions.

The difference between the result of Tsurubuchi *et al.* and those obtained from energy-loss spectroscopy measurements is very pronounced at energies below 50 eV (up to an order of magnitude). These discrepancies and a steep minimum at around 18 eV (not physically justifiable[4]) could be attributed to bad statistics at low energy. Therefore, we omit from our compilation the low-energy data of Tsurubuchi *et al.* The rescaled apparent excitation cross sections of Ajello *et al.* are instead consistent in shape with the energy-loss spectroscopy measurements and are therefore used in our compilation. We interpolated the weighted average of experimental data of both states using Eq. (47) and checked the data consistency in the high-energy range with a Fano plot (Fig. 16). The linear fit for the adopted cross sections yields the following values for the optical oscillator strengths: $f_{1s_2}=0.280\pm0.045$, $f_{1s_4}=0.0769\pm0.0061$.

[4]As pointed out in Sec. III.B, excitation cross sections generally start to have nonzero values at threshold ($T=E_n$), monotonically increase to a maximum value according to some simple power law, and then decrease following the Bethe-Born approximation.

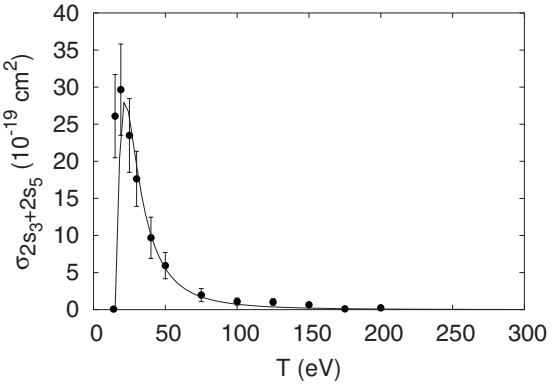

FIG. 20. Sum cross sections for levels $2s_3$ and $2s_5$. The experimental data (●) of Chilton and Lin (1999) are fitted (solid line) with Eq. (47).

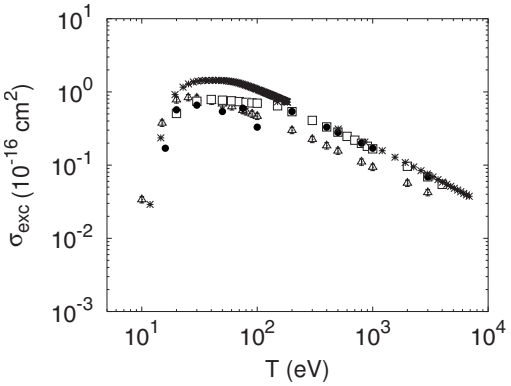

FIG. 21. Comparison between the total excitation cross sections obtained in this work (△) and other compilations: *, Eggarter (1975); □, de Heer *et al.* (1979); ●, Zecca *et al.* (1996).

The agreement with those reported in Table XI is within the stated uncertainties.

The cross sections of levels $3s_1'$ and $3d_2$ were measured only by Chutjian and Cartwright and those of states $2s_2$, $2s_4$, and $3d_5$ (shown in Fig. 17) only by Stewart *et al.* (2002). In contrast to the usual shape for optically allowed states, the cross section for transitions into level $3d_5$ presents a sharp peak near the threshold. This can be explained theoretically by a very small singlet *LS* component in the wave function (Stewart *et al.*, 2002; Weber *et al.*, 2004).

2. Optically forbidden states

The excitation cross-section values for the metastable levels $1s_3$ and $1s_5$ are about one order of magnitude smaller than those of the resonance levels $1s_2$ and $1s_4$ (see Fig. 18). The results obtained for level $1s_3$ by Filipović *et al.* (2000b) and Khakoo *et al.* (2004) using energy-loss spectroscopy and by Schappe *et al.* (1994) with optical methods match within 40% at low energies, while the values of Chutjian and Cartwright (1981) are systematically lower. Therefore, we did not use these data to calculate the weighted mean.

The most extensive study concerning the $4p$ states was conducted by Chilton *et al.* (1998), whose results we used for the data compilation. Figure 19 illustrates the sum of the cross sections for states $2p_1$–$2p_{10}$. The values of Chutjian and Cartwright are compatible with those of Chilton *et al.* within the overall uncertainty, apart from the point at 100 eV. The data retrieved from the IAEA database (see Sec. I.A) and those adopted by Eggarter and Hayashi are also shown for comparison.

The sum cross section for the two levels $2s_3$ and $2s_5$ can be seen in Fig. 20. For these levels, the only experimental data are those of Chilton and Lin (1999).

3. Comparison with earlier data on total excitation

Figure 21 shows our adopted total excitation cross

TABLE VI. Most relevant work on electron ionization cross sections for Ar.

Author	Technique	Type	Energy range (eV)
Rapp and Englander-Golden, 1965	Condenser plate[a]	Total	Threshold–1000
Wetzel *et al.*, 1987	Crossed beam[b]	σ_i^{n+}, $n=1,2$	0–200
Krishnakumar and Srivastava, 1988	Static gas[c]	σ_i^{n+}, $n=1,\ldots,3$	Threshold–1000
Ma *et al.*, 1991	Crossed beam[c]	σ_i^{n+}, $n=1,2$	Threshold–500
Syage, 1991	Crossed beam[d]	σ^{n+}, $n=1,\ldots,3$	0–660
McCallion *et al.*, 1992	Crossed beam[c]	σ_i^{n+}, $n=1,\ldots,5$	Threshold–5300
Straub *et al.*, 1995	Condenser plate (q/M discrimination)[b]	σ^{n+}, $n=1,\ldots,4$	Threshold–1000
Sorokin *et al.*, 2000	Static beam[e]	Total	140–4000
Rejoub *et al.*, 2002	Condenser plate (q/M discrimination)[b]	σ^{n+}, $n=1,2$	Threshold–1000

[a]Relative to H_2.
[b]Absolute.
[c]Relative to Rapp and Englander-Golden, 1965.
[d]Relative to an average value of σ^+.
[e]Relative to photoionization measurements.

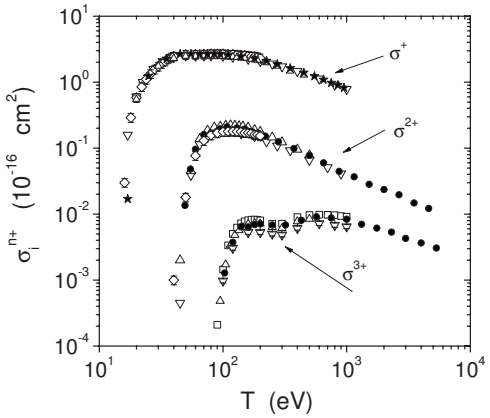

FIG. 22. Cross sections for single, double, and triple ionization. ▽, Rejoub *et al.* (2002); ◇, Wetzel *et al.* (1987); △, Ma *et al.* (1991); ⋆, Straub *et al.* (1995); ●, McCallion *et al.* (1992); □, Krishnakumar and Srivastava (1988).

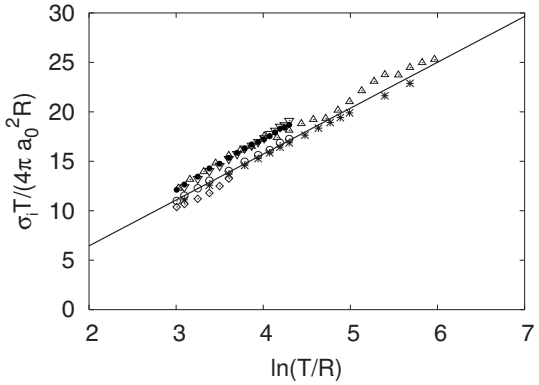

FIG. 24. Fano plot of the total ionization cross-section data for argon. ▽, Rapp and Englander-Golden (1965); ◇, Ma *et al.* (1991); △, McCallion *et al.* (1992); ●, Straub *et al.* (1995); ○, Rejoub *et al.* (2002); *, Sorokin *et al.* (2000). Solid line: linear fit of the adopted data set.

section in comparison with those of other data from the literature. The compilation of Zecca *et al.* (1996) is based on the work of de Heer *et al.* (1979) and Chutjian and Cartwright (1981). These data were also selected by Inokuti *et al.* (2000) for their compilation. Our data improve the cross-section values, especially at energies above 100 eV.

D. Ionization cross sections

In Table VI, we list significant ionization cross sections for argon. The data from Rapp and Englander-Golden (1965), consisting of total ionization cross sections measured in the energy range between threshold and 1 keV, are relative to hydrogen data and have an overall uncertainty of about 7%. Many (e.g., Krishnakumar and Srivastava, 1988; McCallion *et al.*, 1992) referred to these data to calibrate their apparatus. Wetzel *et al.* (1987) used a crossed-beam technique to measure the absolute value of σ_i^+ at the peak energy with an uncertainty of 17%. They obtained the single- and double-ionization cross sections in the energy range from threshold to 200 eV by means of relative measurements. Krishnakumar and Srivastava (1988) obtained multiple-ionization cross-section data in the energy range from threshold up to 1 keV using the relative-flow technique with an overall uncertainty of 10% for single-ionization, 13% for double-ionization, and 19% for triple-ionization data. Possible uncertainties may arise from electron current measurements, pressure measurements, change in the path length, and space charge effects. Ma *et al.* (1991) provided relative measurements of single- and double-ionization cross sections on the basis of an absolute evaluation of the single-ionization cross section at $T=80$ eV by means of time-of-flight measurements with a pulsed electron beam source. The same technique was used by others either with a static atomic beam (Straub *et al.*, 1995) or with a crossed beam (Syage, 1991, McCallion *et al.*, 1992). The uncertainties inherent in this method are due to errors in the ion ratio measurements, in the determination of the cross-section shape, and in the normalization procedure.

Figures 22 and 23 show a selection of relevant data for single, double, triple, and total ionization. We constructed the adopted sets using a weighted mean of all

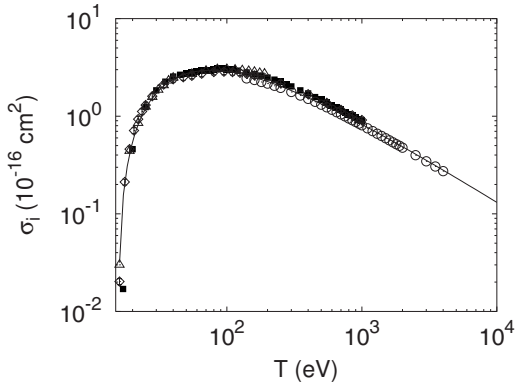

FIG. 23. Total ionization cross section. The solid line represents the interpolation function of the adopted set, according to Eq. (49), with $b=(3.66\pm0.11)\times10^{-3}$, $c=(1.43\pm4.88)\times10^{-4}$, $d=(6.76\pm0.74)\times10^{-3}$. For clarity, only the experimental data of Straub *et al.* (1995) (■), Sorokin *et al.* (2000) (○), Wetzel *et al.* (1987) (△), and Rapp and Englander-Golden (1965) (◇) are shown.

TABLE VII. Slopes of Fano plots for total ionization cross sections for argon, according to Eqs. (14) and (15).

Author	M_i^2
Rapp and Englander-Golden, 1965	5.498±0.047
Ma *et al.*, 1991	4.68±0.35
McCallion *et al.*, 1992	4.39±0.09
Straub *et al.*, 1995	5.022±0.057
Sorokin *et al.*, 2000	4.485±0.026
Rejoub *et al.*, 2002	4.811±0.062
Adopted set	4.641±0.056

TABLE VIII. Available differential ionization cross sections for Ar.

Author	Incident electron energy T (eV)	Ejected electron energy (eV)	Ejected electron angle θ
Santos *et al.*, 2003	500, 750, 1000	0.15 $T-T$	$-22° < \theta < 22°$
Schmitt *et al.*, 1994	100	15	$0° < \theta < 90°$
Chaudry *et al.*, 1989	$5\times10^2-10^4$	20–270	90°
DuBois and Rudd, 1978	100–500	$4-(T-B_1)$	$10° < \theta < 150°$
Vroom *et al.*, 1977	10^3-10^4	50–200	30°, 60°, …, 150°
Mathis and Vroom, 1976	1000	4–500	90°
Opal *et al.*, 1972	500	4–200	$30° < \theta < 150°$

available data since there was general agreement within the reported uncertainty. For the total cross section, we interpolated the adopted data using Eq. (49), and analyzed the high-energy dependence with a Fano plot (see Fig. 24). The results of the linear fits relative to the Fano plots are reported in Table VII and show a maximum discrepancy of about 13% (excluding the data of Rapp and Englander-Golden, which differ by about 18% from the average value). Moreover, the slope of our adopted set is in agreement with the value $M^2_{\text{tot}}=4.330$ obtained from Eq. (51) with $\mu=-1$. This confirms the physical consistency of the ionization cross-section data at high impact energy.

1. Differential ionization cross sections

The single- and double-differential cross sections (SDCSs and DDCSs) for ionization in Ar have been measured in a few experiments (see Table VIII), even though these data provide information on the energy spectrum and spatial distribution of secondary electrons in an irradiated medium. It is therefore difficult to evaluate this poor set of data or to attempt comparisons with theoretical works, in particular in the case of DDCSs.

In Fig. 25 we present some representative data on the DDCSs. For $\theta=90°$, there is general agreement at secondary-electron energies below 200 eV; it is, however, difficult to draw any conclusion above 200 eV, given the paucity of the data. DDCSs at low ejection angles were measured only by DuBois and Rudd (1978) ($\theta\geqslant12°$) and Santos *et al.* (2003) ($\theta=0°$); therefore, also in this case, it is difficult to judge the quality of the data.

We show in Fig. 26 the SDCSs for impact energies $T=500$ eV and 1 keV and the respective BEB functions [see Eq. (43) and Table X]. These curves were obtained after fitting the oscillator strength distribution df/dw with the function $y(w)=A/(1+w)^2$. The good agreement with the BEB approximation confirms the physical consistency of the data, obtained with two independent methods (cross sections and oscillator strengths). Figure 27 shows the SDCSs in the form of a Platzman plot. The shape of $Y(E)$ [see Eq. (50)] at $T=1$ keV is consistent with that of $E(df/dE)$ for slow secondary electrons, while at $T=500$ eV more data are necessary to confirm this statement.

2. *K*-shell ionization

Accurate inner-shell ionization cross sections by electron impact are required in many fields of material analysis, such as Auger-electron spectroscopy, electron probe microanalysis, and x-ray fluorescence spectros-

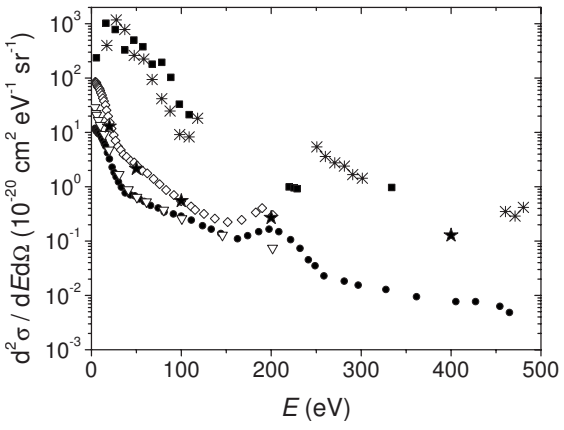

FIG. 25. Available DDCS data for electron ionization in argon. $T=500$ eV: ■, Santos *et al.* (2003) ($\theta=0°$); ◇, Opal *et al.* (1972) ($\theta=90°$); ★, DuBois and Rudd (1978) ($\theta=90°$). $T=1$ keV: ●, Mathis and Vroom (1976) ($\theta=90°$); ▽, Vroom *et al.* (1977) ($\theta=90°$); *, Santos *et al.* (2003) ($\theta=0°$).

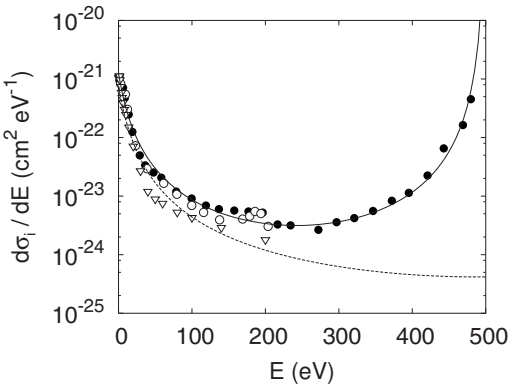

FIG. 26. Available SDCS data for electron ionization in argon. $T=500$ eV: ○, Opal *et al.* (1972); ●, DuBois and Rudd (1978); $T=1$ keV: ▽, Vroom *et al.* (1977). Solid and dashed lines: BEB approximations, with $df/dw=A/(1+w)^2$, $A=0.411\pm0.028$.

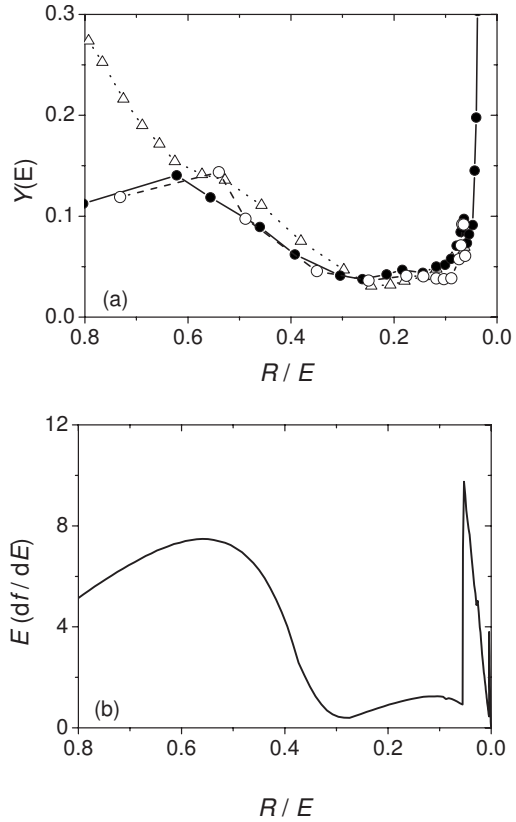

FIG. 27. Platzman plot of SDCS cross sections of Ar shown in Fig. 26 for (a) electron ionization and (b) photoionization. $Y(E)$ is the scaled SDCS, according to Eq. (50). $T=500$ eV: ○, Opal *et al.* (1972); ●, DuBois and Rudd (1978); $T=1$ keV: △, Vroom *et al.* (1977). E is (a) the electron energy or (b) the photon impact energy.

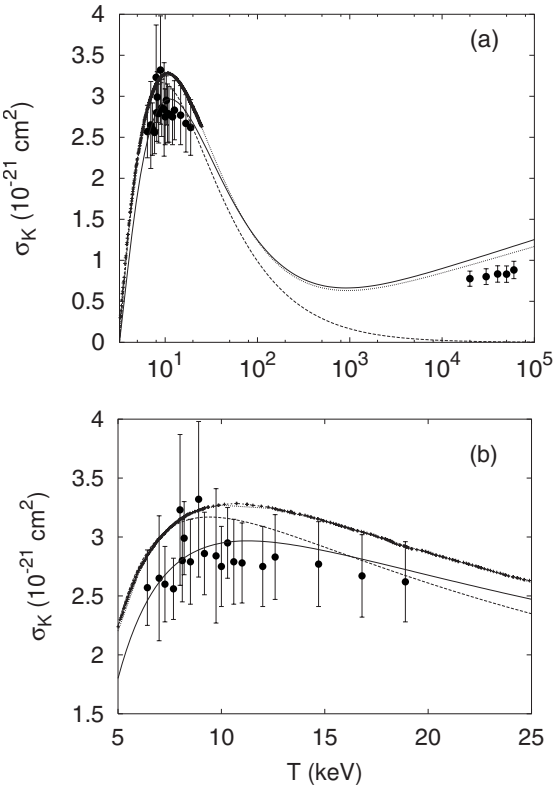

FIG. 28. K-shell ionization cross section for argon in the energy range (a) 1keV–100 MeV and (b) 5–25 keV. ●, compilation provided by Liu *et al.* (2000). Calculations: solid line, BEB approximation (Kim *et al.*, 2000); dotted line, Bote and Salvat (2007); (+), Segui *et al.* (2003). Semiempirical evaluation: dashed line, Casnati *et al.* (1982).

copy. Moreover, there is demand for coherent data for Monte Carlo simulations of radiation transport in matter, with applications in astrophysics, detector response studies, and radiotherapy. The common techniques for measuring inner-shell ionization cross sections are electron energy-loss spectroscopy (see Fig. 2), photoionization, and analysis of characteristic x rays. However, cross-section data are still incomplete. For example, argon cross sections for K-shell ionization by electron impact are still lacking in the energy range 100 keV–10 MeV (Liu *et al.*, 2000). Many efforts have been made in recent years to collect more data and to provide a satisfactory theoretical analysis (Kim *et al.*, 2000; Segui *et al.*, 2003; Bartlett and Stelbovics, 2004). Gryzinski (1965) and Casnati *et al.* (1982), among others, suggested simple equations to describe K-shell ionization cross sections. In Fig. 28, we show the compilation of Liu *et al.* for the K-shell ionization cross section σ_K as compared with theoretical results and a semiempirical evaluation according to the nonrelativistic formula of Casnati *et al.* As the DWBA partial-wave series described by Segui *et al.* converges only for projectiles with energies up to about ten times the ionization threshold, Bote and Salvat (2007) developed a model that introduces empirical (Coulomb and exchange) corrections to the plane-wave Born approximation (PWBA).

This comparison clearly shows the need for more experimental data to confirm the validity of theoretical models at higher energies ($T \geqslant 100$ keV). Nevertheless,

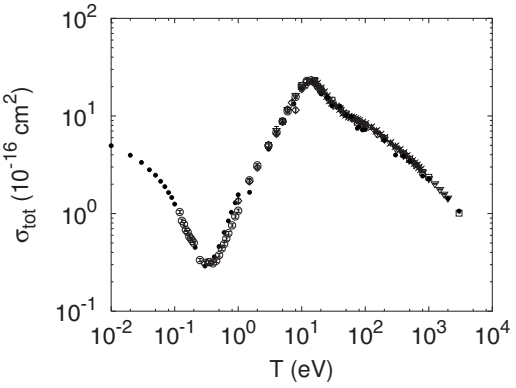

FIG. 29. Comparison between the argon total cross section as a function of the electron energy, obtained by adding the inelastic and elastic cross sections adopted in this work (●), and independent measurements of the total scattering cross section: *, Wagenaar and de Heer (1985); ▽, Baek and Grosswendt (2003); ◇, Taihua *et al.*, (1996); ○, Buckman and Lohmann (1986). The set recommended by Zecca *et al.* (1996) is also shown for comparison (□).

TABLE IX. Argon energy levels, from Ralchenko *et al.*, 2006.

Configuration	Total angular momentum J	Level energy (eV)	Paschen designation
$3p^6$	0	0	$1p_0$
$3p^5 4s$	2	11.548	$1s_5$
	1	11.624	$1s_4$
	0	11.723	$1s_3$
	1	11.828	$1s_2$
$3p^5 4p$	1	12.907	$2p_{10}$
	3	13.076	$2p_9$
	2	13.095	$2p_8$
	1	13.153	$2p_7$
	2	13.172	$2p_6$
	0	13.273	$2p_5$
	1	13.283	$2p_4$
	2	13.302	$2p_3$
	1	13.328	$2p_2$
	0	13.480	$2p_1$
$3p^5 3d$	0	13.845	$3d_6$
	1	13.864	$3d_5$
	4	13.979	$3d'_4$
	3	14.013	$3d_4$
	2	13.903	$3d_3$
	1	14.153	$3d_2$
	2	14.063	$3d''_1$
	3	14.099	$3d'_1$
	2	14.214	$3s'''_1$
	3	14.236	$3s'''_1$
	2	14.234	$3s''_1$
	1	14.304	$3s'_1$
$3p^5 5s$	2	14.068	$2s_5$
	1	14.090	$2s_4$
	0	14.241	$2s_3$
	1	14.255	$2s_2$
$3p^5 4d$	0	14.694	$4d_6$
	1	14.711	$4d_5$
	2	14.743	$4d_3$
	1	14.859	$4d_2$
	4	14.757	$4d'_4$
	3	14.781	$4d_4$
	2	14.809	$4d''_1$
	3	14.824	$4d'_1$
	2	14.953	$4s'''_1$
	1	15.004	$4s'_1$
	2	14.955	$4s''_1$
	3	14.972	$4s'''_1$
$3p^5 6s$	2	14.839	$3s_5$
	1	14.848	$3s_4$
	0	15.014	$3s_3$
	1	15.022	$3s_2$
$3p^5 5d$	0	15.101	$5d_6$
	1	15.118	$5d_5$
	4	15.131	$5d'_4$
	3	15.146	$5d_4$
	2	15.137	$5d_3$
	1	15.190	$5d_2$
	2	15.161	$5d''_1$
	3	15.167	$5d'_1$
$3p^5 7s$	2	15.181	$4s_5$
	1	15.186	$4s_4$
$3p^5 6p$	1	15.202	$4p_{10}$
	2	15.186	$4p_9$

the relativistic-BEB approximation agrees well with the PWBA calculation of Bote and Salvat and provides a fair estimate of the available data over the whole energy range. Therefore, this approximation can be used to implement the K-shell cross section in electron transport calculations.

E. Total scattering cross section

Our integrated cross sections for elastic, excitation, and ionization processes were summed to obtain the argon total cross section, which was then compared with independent experimental data, as shown in Fig. 29. Agreement with the experimental data and with those reported in the earlier compilations of Zecca *et al.* (1996) and Inokuti *et al.* (2000) is within overall stated uncertainties, thus confirming again the consistency of these newly compiled cross sections.

VI. CONCLUDING REMARKS

The compilation of accurate scattering cross sections is of crucial importance not only when modeling electron transport through matter but also for experimental applications in surface and material analysis, or to improve plasma diagnostic techniques, such as optical emission spectroscopy (Boffard *et al.*, 2004). While much effort has been devoted to the improvement of theoretical models describing electron transport and scattering, the update of fundamental data sets on the basis of re-

TABLE X. Binding energies, kinetic energies, and orbital occupation numbers for argon, from Rudd *et al.* (1992).

Orbital	B_i (eV)	U_i (eV)	N_i
1*s*	3202.9	4192.9	2
2*s*	326.0	683.1	2
2*p*	249.18	651.4	6
3*s*	29.24	103.5	2
3*p*	15.82	78.07	6

TABLE XI. Optical oscillator strengths for discrete transitions from ground state in argon (experimental data).

State	f_n	Author	Adopted
$1s_2$	0.207±0.063	Tsurubuchi *et al.*, 1996	
	0.265±0.013	Wu *et al.*, 1995	
	0.2214±0.0068	Gibson and Risley, 1995	
	0.265±0.013	Chan *et al.*, 1992	
	0.222±0.02	Li *et al.*, 1988	
	0.240±0.02	Westerveld *et al.*, 1979	
	0.210±0.030	Vallee *et al.*, 1977	
	0.283±0.024	Copley and Camm, 1974	
	0.35±0.13	Irwin *et al.*, 1973	
	0.22±0.02	de Jongh and van Eck, 1971	
	0.186±0.037	Geiger, 1970	
	0.228±0.021	Lawrence, 1968	
		This work	0.233±0.004
		Eggarter, 1975	0.250
		Berkowitz, 2002	0.2214
$1s_4$	0.052±0.019	Tsurubuchi *et al.*, 1996	
	0.0676±0.0040	Wu *et al.*, 1995	
	0.0580±0.0017	Gibson and Risley, 1995	
	0.0662±0.0033	Chan *et al.*, 1992	
	0.058±0.003	Li *et al.*, 1988	
	0.065±0.005	Chornay *et al.*, 1984	
	0.063±0.005	Westerveld *et al.*, 1979	
	0.051±0.007	Vallee *et al.*, 1977	
	0.076±0.008	Copley and Camm, 1974	
	0.083±0.027	Irwin *et al.*, 1973	
	0.096±0.02	McConkey and Donaldson, 1973	
	0.047±0.009	Geiger, 1970	
	0.059±0.003	Lawrence, 1968	
		This work	0.060±0.001
		Eggarter, 1975	0.0633
		Berkowitz, 2002	0.0580
$3s_1'$	0.106±0.010	Wu *et al.*, 1995	
	0.106±0.011	Chan *et al.*, 1992	
	0.086±0.007	Westerveld *et al.*, 1979	
		This work	0.092±0.006
		NIST[a]	0.106±0.0265
		Eggarter, 1975	0.090
		Berkowitz, 2002	0.106
$3d_2$	0.0929±0.0078	Wu *et al.*, 1995	
	0.0914±0.0091	Chan *et al.*, 1992	
	0.079±0.006	Westerveld *et al.*, 1979	
		This work	0.083±0.005
		NIST	0.0932±0.0233
		Berkowitz, 2002	0.090
$2s_2$	0.009±0.003	Stewart *et al.*, 2002	
	0.0122±0.0032	Wu *et al.*, 1995	
	0.0126±0.0013	Chan *et al.*, 1992	
	0.0106±0.0008	Westerveld *et al.*, 1979	
		This work	0.0110±0.0007

TABLE XI. (*Continued.*)

State	f_n	Author	Adopted
		NIST	0.012±0.003
		Berkowitz, 2002	0.012
$2s_4$	0.027±0.005	Stewart *et al.*, 2002	
	0.0241±0.0029	Wu *et al.*, 1995	
	0.0264±0.0026	Chan *et al.*, 1992	
	0.025±0.002	Westerveld *et al.*, 1979	
		This work	0.0257±0.0015
		NIST	0.027±0.007
		Berkowitz, 2002	0.026
$3d_5$	0.0010±0.0003	Wu *et al.*, 1995	
	0.0013±0.0001	Chan *et al.*, 1992	
	0.00089±0.00007	Westerveld *et al.*, 1979	
		This work	0.00102±0.00006
		Berkowitz, 2002	0.0011
$4d_5$	0.0019±0.0002	Chan *et al.*, 1992	
$3s_4$	0.0144±0.0014		
$4d_2$	0.0484±0.0048		
Sum			0.065±0.005
		Eggarter, 1975	0.060
$4s_1'$	0.0209±0.0021	Chan *et al.*, 1992	
$3s_2$	0.0221±0.0022		
$5d_5$	0.0041±0.0004		
Sum			0.047±0.003
		Eggarter, 1975	0.040
$4s_4$	0.0426±0.0043	Chan *et al.*, 1992	
$5d_2$	0.0426±0.0043		
Sum			0.085±0.006
		Eggarter, 1975	0.030
Total discrete		This work	0.713±0.011
		Berkowitz, 2002	0.8633
		Chan *et al.*, 1992	0.859±0.004
		Eggarter, 1975	0.793

[a]Ralchenko *et al.* (2006).

cent experimental results is often neglected [as discussed by Yanguas-Gil *et al.* (2005)]. Therefore, we considered it opportune and of general interest to review the progress made in the field of experimental electron scattering. Our work contributes to the collection and dissemination of comprehensive and updated cross sections for the argon atom. The use of a well-validated set of electron cross sections ensures the quality of calculated transport parameters and ionization yields, for instance in plasma physics and radiation physics. Another often neglected aspect is the propagation of uncertainties affecting cross-section data to calculated quantities. Consequently, it is desirable to establish procedures to perform sensitivity analysis: How much agreement or disagreement is due to statistical fluctuations? How much is due to intrinsic errors in the adopted data sets? For example, Monte Carlo techniques can be used to study the effect of statistical uncertainties on the calculated quantities [for application in the analysis of low-energy cross sections, see Buckman and Mitroy (1989)]. Using a random number generator, the cross-section values can be varied within their statistical uncertainty, and the new set can be used again to calculate transport parameters or ionization yields in the gas of interest. This method can estimate whether the discrepancies obtained in the results are compatible with the overall uncertainty in the corresponding experimental data. The new set of electron scattering cross sections reported in this work satisfies several consistency requirements that are well established for electron scattering at high impact energies. Moreover, the cross-checking of data obtained from independent experiments ensures that systematic errors are minimized. Much remains to be done, however, at low and intermediate impact energies, where the

discrepancies among experimental data are high and where even widely used theoretical methods still fail to describe the scattering processes (see Secs. V.B and V.C.1).

The new compilation of oscillator strengths and cross sections for argon obtained in this work is also available online at http://www.ptb.de/en/org/6/66/664/index.htm

ACKNOWLEDGMENTS

We are indebted to David Bote and Frances Salvat (Universitat de Barcelona) for providing their results on *K*-shell ionization cross sections before publication. We are grateful to Marcel Reginatto (PTB) for fruitful discussions and critical comments during the preparation of the manuscript. We also thank Heike Nittmann (PTB) for help in manuscript preparation.

APPENDIX A: ARGON ENERGY LEVELS AND BINDING ENERGIES

We report in Table IX the argon energy levels along with the Paschen designation and the value of the total angular momentum J. In Table X, we give the binding energies B_i, the kinetic energies U_i, and the occupation numbers N_i for several orbitals of the argon atom.

APPENDIX B: TABLES FOR OSCILLATOR STRENGTHS

We show, in Table XI, the optical oscillator strengths for discrete transitions from the ground state in argon.

REFERENCES

Ajello, J. M., G. K. James, B. Franklin, and S. Howell, 1990, J. Phys. B **23**, 4355.
Baek, W. Y., and B. Grosswendt, 2003, J. Phys. B **36**, 731.
Bartlett, P. L., and A. T. Stelbovics, 2002, Phys. Rev. A **66**, 012707.
Bartlett, P. L., and A. T. Stelbovics, 2004, At. Data Nucl. Data Tables **86**, 235.
Bederson, B., 1969, Comments At. Mol. Phys. **1**, 41.
Bederson, B., and L. J. Kieffer, 1971, Rev. Mod. Phys. **43**, 601.
Bell, K. L., H. B. Gilbody, J. G. Hughes, A. E. Kingston, and F. J. Smith, 1983, J. Phys. Chem. Ref. Data **12**, 891.
Bell, K. L., N. S. Scott, and M. A. Lennon, 1984, J. Phys. B **17**, 4757.
Berger, M. J., J. H. Hubbell, S. M. Seltzer, J. Chang, J. S. Coursey, R. Sukumar, and D. S. Zucker, 2005, *XCOM: Photon Cross Section Database (Version 1.3)* (National Institute of Standard and Technology, Gaithersburg, MD), available at http://physics.nist.gov/xcom
Berkowitz, J., 2002, *Atomic and Molecular Photoabsorption: Absolute Total Cross Sections*, 2nd ed. (Academic, San Diego).
Boffard, J. B., C. C. Lin, and C. A. DeJoseph, Jr., 2004, J. Phys. D **37**, R143.
Boffard, J. B., G. A. Piech, M. F. Gehrke, L. W. Anderson, and C. C. Lin, 1999, Phys. Rev. A **59**, 2749.
Bote, D., and F. Salvat, 2007, private communication.
Bransden, B. H., and C. J. Joachain, 2003, *Physics of Atoms and Molecules* (Prentice Hall, London).
Bray, I., and D. V. Fursa, 1996, Phys. Rev. Lett. **76**, 2674.
Buckman, S. J., and M. J. Brunger, 1997, Aust. J. Phys. **50**, 483.
Buckman, S. J., and B. Lohmann, 1986, J. Phys. B **19**, 2547.
Buckman, S. J., and J. Mitroy, 1989, J. Phys. B **22**, 1365.
Burke, P. G., 1994, Adv. At., Mol., Opt. Phys. **32**, 117.
Burke, P. G., and K. A. Berrington, 1993, Eds., *Atomic and Molecular Processes: An R-Matrix Approach* (Institute of Physics, Bristol).
Cartwright, D. C., A. Chutjian, S. Trajmar, and W. Williams, 1977, Phys. Rev. A **16**, 1013.
Casnati, E., A. Tartari, and C. Baraldi, 1982, J. Phys. B **15**, 155.
Chan, W. F., G. Cooper, and C. E. Brion, 1991, Phys. Rev. A **44**, 186.
Chan, W. F., G. Cooper, X. Guo, G. R. Burton, and C. E. Brion, 1992, Phys. Rev. A **46**, 149.
Chantler, C. T., K. Olsen, R. A. Dragoset, J. Chang, A. R. Kishore, S. A. Kotochigova, and D. S. Zucker, 2005, *X-Ray Form Factor, Attenuation and Scattering Tables (Version 2.1)* (National Institute of Standard and Technology, Gaithersburg, MD), available at http://physics.nist.gov/ffast
Chaudry, M. A., A. J. Duncan, R. Hippler, and H. Kleinpoppen, 1989, Phys. Rev. A **39**, 530.
Chilton, J. E., J. B. Boffard, R. S. Schappe, and C. C. Lin, 1998, Phys. Rev. A **57**, 267.
Chilton, J. E., and C. C. Lin, 1999, Phys. Rev. A **60**, 3712.
Chornay, D. J., G. C. King, and S. J. Buckman, 1984, J. Phys. B **17**, 3173.
Chutjian, A., and D. C. Cartwright, 1981, Phys. Rev. A **23**, 2178.
Cooper, J. W., 2000, *Landolt-Böernstein Numerical Data and Functional Relationships in Science and Technology, New Series, Group I* (Springer, Berlin), Vol. 17A, Chap. 1, pp. 1–82.
Copley, G. H., and D. M. Camm, 1974, J. Quant. Spectrosc. Radiat. Transf. **14**, 899.
Crompton, R. W., 1994, Adv. At., Mol., Opt. Phys. **33**, 97.
Cvejanović, D., and A. Crowe, 1997, J. Phys. B **30**, 2873.
de Heer, F. J., R. H. J. Jansen, and W. van der Kaay, 1979, J. Phys. B **12**, 979.
de Jongh, J. P., and J. van Eck, 1971, Physica (Amsterdam) **51**, 104.
Doolen, G., and D. A. Liberman, 1987, Phys. Scr. **36**, 77.
DuBois, R. D., and M. E. Rudd, 1976, J. Phys. B **9**, 2657.
DuBois, R. D., and M. E. Rudd, 1978, Phys. Rev. A **17**, 843.
Eggarter, E., 1975, J. Chem. Phys. **62**, 833.
Fano, U., 1954, Phys. Rev. **95**, 1198.
Fano, U., and J. W. Cooper, 1968, Rev. Mod. Phys. **40**, 441.
Filipović, D. M., B. P. Marinković, V. Pejčev, and L. Vušković, 2000a, J. Phys. B **33**, 677.
Filipović, D. M., B. P. Marinković, V. Pejčev, and L. Vušković, 2000b, J. Phys. B **33**, 2081.
Filippelli, A. R., C. C. Lin, L. W. Anderson, and J. W. McConkey, 1994, Adv. At., Mol., Opt. Phys. **33**, 1.
Fite, W. L., and R. T. Brackmann, 1958, Phys. Rev. **112**, 1141.
Froome, K. D., 1955, Proc. Phys. Soc. London, Sect. B **68**, 833.
Frost, L. S., and A. V. Phelps, 1964, Phys. Rev. **136**, A1538.
Furst, J. E., D. E. Golden, M. Mahgerefteh, J. Zhou, and D. Mueller, 1989, Phys. Rev. A **40**, 5592.
Gallagher, J. W., 1994, Adv. At., Mol., Opt. Phys. **33**, 373.
Gallagher, J. W., C. E. Brion, J. A. R. Samson, and P. W. Langhoff, 1988, J. Phys. Chem. Ref. Data **17**, 9.

Geiger, J., 1970, Phys. Lett. **33A**, 351.
Gibson, J. C., R. J. Gulley, J. P. Sullivan, S. J. Buckman, V. Chan, and P. D. Burrow, 1996, J. Phys. B **29**, 3177.
Gibson, N. D., and J. S. Risley, 1995, Phys. Rev. A **52**, 4451.
Green, A. E. S., and C. A. Barth, 1965, J. Geophys. Res. **70**, 1083.
Grosswendt, B., and W. Y. Baek, 2000, *Radiation Quality Assessment Based on Physical Radiation Interaction at Nanometer Level—LNL-INFN-Report 161* (Laboratori Nazionali di Legnaro, Padova, Italy), Chap. 1, p. 5.
Gryzinski, M., 1965, Phys. Rev. **138**, A336.
Gryzinski, M., and J. A. Kunc, 2000, J. Phys. B **33**, 1549.
Haddad, G. N., and T. F. O'Malley, 1982, Aust. J. Phys. **35**, 35.
Hayashi, M., 2003, *Bibliography of Electron and Photon Cross Sections with Atoms and Molecules Published in the 20th Century: Argon*, Technical Report NIFS-DATA-72 (National Institute for Fusion Science, Toki, Japan).
Heddle, D. W. O., and J. W. Gallagher, 1989, Rev. Mod. Phys. **61**, 221.
Henke, B. L., E. M. Gullikson, and J. C. Davis, 1993, At. Data Nucl. Data Tables **54**, 181.
Hyder, G. M. A., M. S. Dababneh, Y. F. Hsieh, W. E. Kauppila, C. K. Kwan, M. Mahdavi-Hezaveh, and T. S. Stein, 1986, Phys. Rev. Lett. **57**, 2252.
ICRU, 1996, *Secondary Electron Spectra from Charged Particle Interactions—Report 55* (International Commission on Radiation Units and Measurements, Bethesda, MD).
Iga, I., L. Mu-Tao, J. C. Nogueira, and R. S. Barbieri, 1987, J. Phys. B **20**, 1095.
Inokuti, M., 1971, Rev. Mod. Phys. **43**, 297.
Inokuti, M., M. T. Elford, S. J. Buckman, and H. Tawara, 2000, *Landolt-Böernstein Numerical Data and Functional Relationships in Science and Technology, New Series, Group I* (Springer, Berlin), Vol. 17A, Chap. 2, pp. 1–81.
Irwin, D., A. E. Livingston, and J. A. Kernahan, 1973, Nucl. Instrum. Methods **110**, 111.
Jablonski, A., F. Salvat, and C. J. Powell, 2002, *NIST Electron Elastic-scattering Cross Section Database—Version 3.0* (National Institute of Standard and Technology, Gaithersburg, MD).
Jablonski, A., F. Salvat, and C. J. Powell, 2004, J. Phys. Chem. Ref. Data **33**, 409.
Jansen, R. H. J., F. J. de Heer, H. J. Luyken, B. van Wingerden, and H. J. Blaauw, 1976, J. Phys. B **9**, 185.
Jasuński, M., P. Jøorgensen, and A. Rizzo, 1995, Theor. Chim. Acta **90**, 291.
Kallman, T. R., and P. Palmeri, 2007, Rev. Mod. Phys. **79**, 79.
Kaveeshwar, V. G., R. Klingbeil, and R. P. Hurst, 1976, Phys. Rev. A **14**, 882.
Khakoo, M. A., P. Vandeventer, J. G. Childers, I. Kanik, C. J. Fontes, K. Bartschat, V. Zeman, D. H. Madison, S. Saxena, R. Srivastava, and A. D. Stauffer, 2004, J. Phys. B **37**, 247.
Kieffer, L. J., and G. H. Dunn, 1966, Rev. Mod. Phys. **38**, 1.
Kim, Y. K., 1975, Radiat. Res. **61**, 21.
Kim, Y. K., 2001, Phys. Rev. A **64**, 032713.
Kim, Y. K., and M. E. Rudd, 1994, Phys. Rev. A **50**, 3954.
Kim, Y. K., J. P. Santos, and F. Parente, 2000, Phys. Rev. A **62**, 052710.
Krishnakumar, E., and S. K. Srivastava, 1988, J. Phys. B **21**, 1055.
Lawrence, G. M., 1968, Phys. Rev. **175**, 40.
Li, G. P., T. Takayanagi, K. Wakiya, H. Suzuki, T. Ajiro, S. Yagi, S. S. Kano, and H. Takuma, 1988, Phys. Rev. A **38**, 1240.
Liu, M., Z. An, C. Tang, Z. Luo, X. Peng, and X. Long, 2000, At. Data Nucl. Data Tables **76**, 213.
Ma, C., C. R. Sporleder, and R. A. Bonham, 1991, Rev. Sci. Instrum. **62**, 909.
Macrossan, M. N., and C. R. Lilley, 2003, Phys. Fluids **15**, 3452.
Märk, T. D., Y. Hatano, and F. Linder, 1995, *Atomic and Molecular Data for Radiotherapy and Radiation Research. Final Report of a Co-ordinated Research Programme—IAEA-TECDOC-799* (International Atomic Energy Agency, Vienna), Chap. 3, p. 163.
Marr, G. V., and J. B. West, 1976, At. Data Nucl. Data Tables **18**, 497.
Mathis, R. E., and D. A. Vroom, 1976, J. Chem. Phys. **64**, 1146.
McCallion, P., M. B. Shah, and H. B. Gilbody, 1992, J. Phys. B **25**, 1061.
McConkey, J. W., and F. G. Donaldson, 1973, Can. J. Phys. **51**, 914.
McDaniel, E. W., and E. J. Mansky, 1994, Adv. At., Mol., Opt. Phys. **33**, 389.
McEachran, R. P., and A. D. Stauffer, 1983, J. Phys. B **16**, 4023.
McEachran, R. P., and A. D. Stauffer, 1997, Aust. J. Phys. **50**, 511.
Mielewska, B., I. Linert, G. C. King, and M. Zubek, 2004, Phys. Rev. A **69**, 062716.
Moiseiwitsch, B. L., and S. J. Smith, 1968, Rev. Mod. Phys. **40**, 238.
Nahar, S. N., and J. M. Wadehra, 1987, Phys. Rev. A **35**, 2051.
Nahar, S. N., and J. M. Wadehra, 1991, Phys. Rev. A **43**, 1275.
Nakamura, Y., and M. Kurachi, 1988, J. Phys. D **21**, 718.
O'Malley, T. F., 1963, Phys. Rev. **130**, 1020.
Opal, C. B., E. C. Beaty, and W. K. Peterson, 1972, At. Data **4**, 209.
Panajotović, R., D. Filipović, B. Marinković, V. Pejčev, M. Kurepa, and L. Vušković, 1997, J. Phys. B **30**, 5877.
Paretzke, H. G., 1989, *Simulation von Elektronenspuren im Energiebereich 0,01–10 keV in Wasserdampf*, Technical Report 24/88, Gesellschaft fuer Strahlen-und Umweltforschung mbH München.
Petrović, Z. L., T. F. O'Malley, and R. W. Crompton, 1995, J. Phys. B **28**, 3309.
Piech, G. A., J. B. Boffard, M. F. Gehrke, L. W. Anderson, and C. C. Lin, 1998, Phys. Rev. Lett. **81**, 309.
Pitchford, L. C., S. V. ONeil, and J. R. Rumble, 1981, Phys. Rev. A **23**, 294.
Puech, V., and L. Torchin, 1986, J. Phys. D **19**, 2309.
Ralchenko, Y., F. C. Jou, D. E. Kelleher, A. E. Kramida, A. Musgrove, J. Reader, W. L. Wiese, and K. Olsen, 2006, *NIST Atomic Spectra Database—Version 3.1.0* (National Institute of Standard and Technology, Gaithersburg, MD), available at http://physics.nist.gov/asd3
Rapp, D., and P. Englander-Golden, 1965, J. Chem. Phys. **43**, 1464.
Rejoub, R., B. G. Lindsay, and R. F. Stebbings, 2002, Phys. Rev. A **65**, 042713.
Rudd, M. E., Y. K. Kim, D. H. Madison, and T. J. Gay, 1992, Rev. Mod. Phys. **64**, 441.
Rudge, M. R. H., 1968, Rev. Mod. Phys. **40**, 564.
Salvat, F., 2003, Phys. Rev. A **68**, 012708.
Salvat, F., A. Jablonski, and C. J. Powell, 2005, Comput. Phys. Commun. **165**, 157.
Samson, J. A. R., and L. Yin, 1989, J. Opt. Soc. Am. B **6**, 2326.
Santos, A. C., H. Hasan, T. Yates, and R. D. DuBois, 2003, Phys. Rev. A **67**, 052708.

Schappe, R. S., M. B. Schulman, L. W. Anderson, and C. C. Lin, 1994, Phys. Rev. A **50**, 444.
Schmidt, B., K. Berkhan, B. Götz, and M. Müller, 1994, Phys. Scr., T **T53**, 30.
Schmitt, A., U. Cerny, H. Möller, W. Raith, and M. Weber, 1994, Phys. Rev. A **49**, R5.
Schneider, B. I., 1994, Adv. At., Mol., Opt. Phys. **33**, 183.
Sebastian, A. A., and J. M. Wadehra, 2005, J. Phys. D **38**, 1577.
Segui, S., M. Dingfelder, and F. Salvat, 2003, Phys. Rev. A **67**, 062710.
Sorokin, A. A., L. A. Shmaenok, S. V. Bobashev, B. Möbus, M. Richter, and G. Ulm, 2000, Phys. Rev. A **61**, 022723.
Srivastava, S. K., A. Chutjian, and S. Trajmar, 1975, J. Chem. Phys. **63**, 2659.
Srivastava, S. K., H. Tanaka, A. Chutjian, and S. Trajmar, 1981, Phys. Rev. A **23**, 2156.
Stewart, M. D., J. E. Chilton, J. B. Boffard, and C. C. Lin, 2002, Phys. Rev. A **65**, 032704.
Straub, H. C., P. Renault, B. G. Lindsay, K. A. Smith, and R. F. Stebbings, 1995, Phys. Rev. A **52**, 1115.
Suzuki, I. H., and N. Saito, 2005, Radiat. Phys. Chem. **73**, 1.
Suzuki, M., T. Taniguchi, and H. Tagashira, 1990, J. Phys. D **23**, 842.
Syage, J. A., 1991, J. Phys. B **24**, L527.
Taihua, L., F. Anping, and Y. Yong, 1996, Radiat. Phys. Chem. **48**, 711.
Trajmar, S., and J. W. McConkey, 1994, Adv. At., Mol., Opt. Phys. **33**, 63.
Tsurubuchi, S., T. Miyazaki, and K. Motohashi, 1996, J. Phys. B **29**, 1785.
Vallee, O., P. Ranson, and J. Chapelle, 1977, J. Quant. Spectrosc. Radiat. Transf. **18**, 327.
Vroom, D. A., R. L. Palmer, and J. W. McGowan, 1977, J. Chem. Phys. **66**, 647.
Vušković, L., and M. V. Kurepa, 1976, J. Phys. B **9**, 837.
Wagenaar, R. W., and F. J. de Heer, 1985, J. Phys. B **18**, 2021.
Weber, T., J. B. Boffard, and C. C. Lin, 2003, Phys. Rev. A **68**, 032719.
Weber, T., J. B. Boffard, and C. C. Lin, 2004, Int. J. Mass. Spectrom. **233**, 75.
Westerveld, W. B., T. F. A. Mulder, and J. V. Eck, 1979, J. Quant. Spectrosc. Radiat. Transf. **21**, 533.
Wetzel, R. C., F. A. Baiocchi, T. R. Hayes, and R. S. Freund, 1987, Phys. Rev. A **35**, 559.
Weyhreter, M., B. Barzick, A. Mann, and F. Linder, 1988, Z. Phys. D: At., Mol. Clusters **7**, 333.
Williams, J. F., 1979, J. Phys. B **12**, 265.
Williams, J. F., and B. A. Willis, 1975, J. Phys. B **8**, 1670.
Wu, S. L., Z. P. Zhong, R. F. Feng, S. L. Xing, B. X. Yang, and K. Z. Xu, 1995, Phys. Rev. A **51**, 4494.
Yang, B. X., and J. Kirz, 1987, Appl. Opt. **26**, 3823.
Yanguas-Gil, A., J. Cotrino, and L. L. Alves, 2005, J. Phys. D **38**, 1588.
Zecca, A., G. P. Karwasz, and R. S. Brusa, 1996, Riv. Nuovo Cimento **19**, 1.
Žigman, V. J., and B. S. Milić, 1988, J. Phys. B **21**, 2609.
Zubek, M., N. Gulley, G. C. King, and F. H. Read, 1996, J. Phys. B **29**, L239.